ENGINEERING RESEARCH JOURNAL (ERJ)
Vol. 51 , No. 2 April. 2022, pp.55-82
Journal Homepage: erj.bu.edu.eg

Analytical Study of In-plan and out-of-plan performance of Confined Masonry Building

Mohamed O.R. El-Hariri[a], Amr A.Gamal[a], Mosaad El-Diasity[b], Sayed Salah .H[c]

[a]Professor, Faculty of Engineering at Shoubra, Benha University.

[b]Assistant Professor, Faculty of Engineering at Shoubra, Benha University.

[c]Assistant Lecturer, Faculty of Engineering at Shoubra, Benha University.

Abstract. Confined masonry (CM) is considered one of the popular forms of low-cost and low-rise construction throughout the world. Confined masonry consists of no reinforced masonry walls surrounded by concrete tie-columns, in the vertical direction, and tie-beams, in the horizontal direction. In some countries confined masonry walls may include joint reinforcement. Although confined masonry structures are still a common masonry construction system in several countries, the majority of them are built using plain masonry. All load-bearing walls in confined masonry constructions must be confining on all sides with horizontal and vertical confining elements. The goal of this research is to use a numerical analysis method using ANSYS software package to evaluate the impact of confining elements such as tie-columns, in-plan walls, and out-plan walls on resisting horizontal lateral loads. Finally, results and conclusions were provided from different finite element analysis models of confined masonry buildings with various confining element configurations.

KEYWORDS: Masonry Building, Confined Masonry, Cyclic Loading, and Finite Element.

1. INTRODUCTION

Masonry systems have a wide variety of forms and have been used as structural material for thousands of years. Some very old stone and brick masonry buildings still exist, proving that masonry successfully resists loads and impacts of environment.(E Abdulahad and E Mahmud et al. 2018[1]). Confined masonry (CM) construction has emerged as a building technology that offers an alternative to both unreinforced masonry (URM) and infilled reinforced concrete (RC) frames. (Bonisha Borah1 et al. 2020[2]).

Over the last 100 years, confined masonry construction had been emerged as a building technology that offers an alternative to both URM and RC frame construction. In a multi-story CM building the stiffness is initially equal at all floor levels, however the collapse occurs at the first story level due to high seismic loads, which cause extensive masonry cracking and resulting decrease in the lateral stiffness. This behavior was confirmed by experimental studies (Svetlana Brzev et al 2015 [3]).

A conservative estimate can be made by assuming that the tie-columns are integrated with the masonry wall, thus a cross-sectional area of the CM wall can be calculated by taking wall density (Roberto M., et al. 2011[4]).

J. Martin Leal-Graciano et al. 2020[5] and Mosaad El-Diasity et al. 2015 [6], studied the behavior of the in-plane confined masonry walls with window openings retrofitted with GFRP and subjected to lateral cyclic loading. In general it can be said that GFRP is a feasible retrofitting and repairing manner, not only to restore lateral strength and deformability capacity, but also, increasing them for masonry walls with holes constructed with poor code specifications for confined walls.

The finite element approach has proven to be a reliable tool for calculating stresses and deformations in structure elements during linear

and non-linear loading stages. The stress-strain relationships, failure criteria, and simulation and modelling of elements all play a role in the application of the non-linear finite element (NLFEA) to restricted masonry structures.

Numerous investigations on finite element models of masonry walls and RC infilled frames have been undertaken in the past. (Hemant, et al. 2007 [7]) investigated uniaxial monotonic compressive stress-strain behavior and calculated the modulus of elasticity of bricks, mortar, and masonry to be 300, 200, and 550 times their compressive strengths, respectively, with corresponding curves that helped assign the relationship of these materials in models.

Separated modelling and integrated modelling are two approaches of finite element modelling for masonry constructions made up of bricks and mortar. The former simulates individual bricks and mortar, whereas the latter simulates their integrity. There are two types of separated modelling approaches: the first assumes that brick and mortar are fully integrated and that the element nodes on the contact surface satisfy the continuous displacement requirement. As a result, the degrees of freedom on the contact surface's associated nodes are linked. The other takes into account bond-slip between brick and mortar, which necessitates the use of interface pieces (Huang et al. 2011 [8]).

(Huang et al. 2011[8]) investigated the characteristics and features of masonry using the solid65 element in "ANSYS® [9]" and numerically simulated the shear properties of joints in masonry structures under various vertical loads (fm). When the experimental and numerical findings were compared, the proposed values for shear transfer coefficient for open and closed cracks of the Solid65 element for modelling masonry structures were 0.3 and 0.6, respectively.

The goal of this study is to create 3D finite element models that are capable of capturing the essential response aspects of failure mode shapes and crack patterns for each model and comparing them to the finite element verification model results to conclude the optimum positioning of CM walls in low storey building at seismic resistance.

2.0 Material properties

It was aimed to create 3D finite element models for the tested 3D two-storey structure assembly, at two different loading case studies, that are capable of capturing the essential response aspects of failure mode shapes and crack patterns for each specimen and comparing them to experimental results and previous references to verify them.

The 3D model consists of two storey building, supported on raft foundation. Each story in had two solid walls, one wall perforated with a window opening of size 0.34 x 0.34 m, and one perforated wall with a door opening of size 0.36 x 0.64 m.

Two different loading case studies were tried. Both cases, S-01-FEM and S-02-FEM, were loaded differed in orientation with respect to loading direction. S-01-FEM was oriented in such a way that loading was imposed perpendicular to the side of specimens with door perforations. Comparatively, S-02-FEM was loaded on the solid wall side to test the effect of openings on the lateral load resistance of the model. The cyclic displacement protocol is shown at Figure 1.

2.1 Theoretical Description of Elements

A computer package called "ANSYS® [9]" was used to do the non-linear finite element analysis. To model the concrete and bricks (SOLID65), an 8-node solid element with three translational and additional rotational degrees of freedom at each node was used, whilst the steel rebar's were modelled using a 2-node bar element (LINK8).

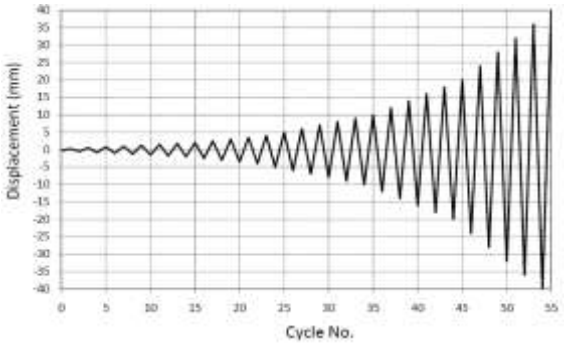

Fig. 1. Cyclic displacement protocol

Within each element, SOLID65 allows for the presence of up to four different materials: one matrix material (e.g. concrete) and up to three independent reinforcing materials. In addition to

combining plastic and creep behavior, the concrete material is capable of directed integration point cracking and crushing. The reinforcement has only uniaxial stiffness and is considered to be spread throughout the element (it also comprises creep and plasticity). Angles set by the user are used to achieve directional alignment.

Link 8 is an engineering spar that can be utilized in a variety of applications. The element can be thought of as a truss element, a cable element, a link element, a spring element, and so on, depending on the application. The three-dimensional spar element is a tension-compression uniaxial element with three degrees of freedom at each node: nodal x, y, and z translations. No bending of the element is taken into account, as it is in a pin-jointed structure. Plasticity, creep, swelling, stress stiffening, and significant deflection capabilities are all part of the package.

SHELL43 excels at simulating linear, distorted, somewhat thick shell structures. At each node, the element has six degrees of freedom: translations in the x, y, and z directions, as well as rotations around the x, y, and z axes. In both in-plane directions, the deformation shapes are linear. It employs a mixed interpolation of tensorial components for out-of-plane motion. Plasticity, creep, stress stiffening, large deflection, and huge strain capacities are all features of this element.

2.2 Material Modeling

A Material idealization and material characteristics are extremely important in nonlinear analysis .

The capacity to forecast the failure of brittle materials is a feature of the concrete material model assigned to the Solid65 element used throughout this work. The failure modes of cracking and crushing are also taken into account. The criterion for concrete failure owing to a multi axial stress state is as follows:

$$\frac{F}{f_c} - S \geq 0 \qquad \text{(Eq. 1)}$$

where:

F = a function of the principal stress state;σxp, σyp, σzp;

fc= uniaxial crushing strength;

S = failure surface expressed in terms of principal stresses and the strength;

parameters ft,fc,fcb,f1 and f2;

ft = ultimate uniaxial tensile strength;

fc = ultimate uniaxial compressive strength;

fcb= ultimate biaxial compressive strength;

f1 = ultimate compressive strength for a state of biaxial compression superimposed on hydrostatic stress state;

f2 = ultimate compressive strength for a state of uniaxial compression

Super imposed on hydrostatic stress state.

Both the function F and the failure surface S are expressed in terms of principal stresses denoted as σ_1 , σ_2 and σ_3 where $\sigma_1 = max(\sigma_{xp}, \sigma_{yp}, \sigma_{zp})$, $\sigma_3 = min(\sigma_{xp}, \sigma_{yp}, \sigma_{zp})$, and $\sigma_1 \geq \sigma_2 \geq \sigma_3$.

The failure of concrete is categorized into four domains:

$0 \geq \sigma_1 \geq \sigma_2 \geq \sigma_3$ (compression–compression-compression)

$\sigma_1 \geq 0 \geq \sigma_2 \geq \sigma_3$ (tensile-compression- compression)

$\sigma_1 \geq \sigma_2 \geq 0 \geq \sigma_3$ (tensile - tensile - compression)

$\sigma_1 \geq \sigma_2 \geq \sigma_3 \geq 0$ (tensile - tensile - tensile)

Independent functions describe the function F and the failure surface S for each domain. F1, F2, F3, and F4 are the four functions that describe the general function F, while S1, S2, S3, and S4 are the four functions that describe S. Figure 2 depicts the failure surface as a 3-D failure surface in principal stress space. The relative magnitudes of the primary stresses are described by the angle of similarity. The 3-D failure surface for biaxial or nearly biaxial stress states is represented by the failure surface in primary stress space with nearly biaxial stress, as shown in Figure 3. If the most significant non-zero principal stresses are in the σxp and σyp directions, the three surfaces presented are for σzp slightly greater than zero, σzp equal to zero, and σzp slightly less than zero. Although the three surfaces, shown as projections on the σxp - σyp plane, are nearly equivalent and the 3-D failure surface is continuous, the mode of material failure is a function of the sign of σzp. For

example, if σxp and σyp are both negative and σzp is slightly positive, cracking would be predicted in a direction perpendicular to the σzp direction. However, if σzp is zero or slightly negative, the material is assumed to crush.

Input strength parameter sft, fc, fcb, f1 and f2 are needed to define the failure surface as well as an ambient hydrostatic stress state. The ultimate uniaxial compressive strength fc, was taken 20 MPa based on the studied bar frame by Mehrabi et. al. (1996) and ft was taken as recommended by ACI specifications, (ft= 0.1 fc).The other parameters were taken as.

fcb= 1.2 fc, f1= 1.45 fc, and f2= 1.725 fc (Eq.2)

Shear transfer coefficients typically range from 0.0 to 1.0, with zero indicating a very smooth fracture (total loss of shear transfer) and 1.0 indicating a very rough crack (no loss of shear transfer). Both the open and closed cracks can benefit from this feature. The open crack shear transfer coefficient was 0.6, and the closed crack shear transfer coefficient was 0.8. The analysis took into account a stress relaxation after cracking value of 0.3. According to various trail experiments, these values provide better performance for the frame load-deflection curve.

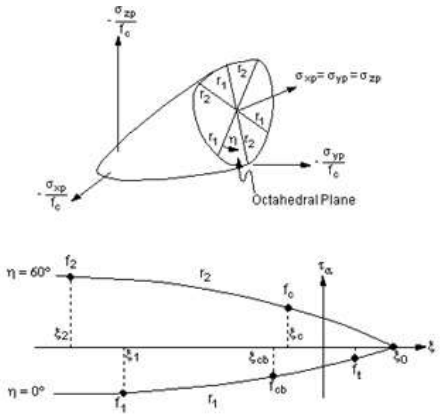

Fig. 2. Failure Surface in Principal Stress Space

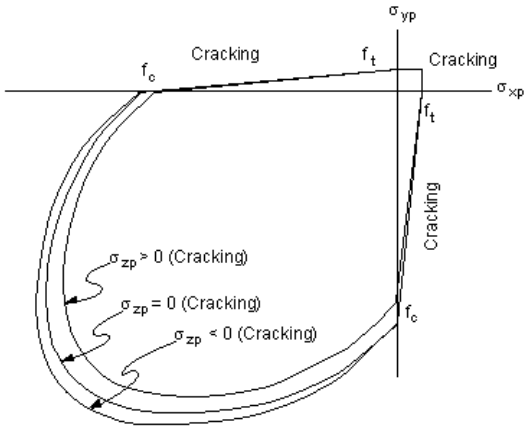

Fig .3. Failure Surface in Principal Stress Space with Nearly Biaxial Stress

.

In modeling of steel reinforcement, the stress-strain connection is represented by two straight lines, as provided by Taijum Wang [2001]. Figure 4 shows the average stress-strain curve of steel bars implanted in concrete

For $\varepsilon_s \le \varepsilon_n$

$$f_s = E_s \varepsilon_s \qquad \text{(Eq. 3)}$$

and for $\varepsilon_s \ge \varepsilon_n$

$$f_s = f_y \left[(0.91 - 2B) + \left(0.02 + 0.25B \frac{\varepsilon_s}{\varepsilon_y} \right) \right] \qquad \text{(Eq. 4)}$$

where fs and εs are the average stress and strain of steel bars, respectively; fy and εy are the yield stress and strain of steel bars, respectively; Es is the young's modulus of steel reinforcement; and $\varepsilon_n = \varepsilon_y (0.93 - 2B)$. The parameter B is given as $\left(f_{cr} / f_y \right)^{1.5} / \rho$, with ρ is the reinforcement ratio, and fcr is the cracking strength of concrete. The recommended value of fcris given as.

$$f_{cr} = 0.31\sqrt{f_c'} \text{ .in MPa} \qquad \text{(Eq. 5)}$$

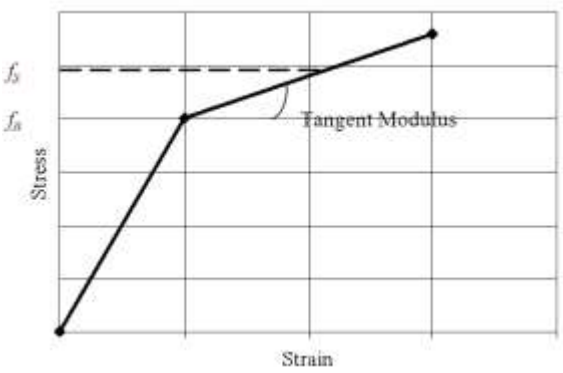

Fig. 4. Modeling of Steel Using Bilinear Kinematic Hardening

The capacity to forecast the failure of brittle materials is a feature of the masonry material model assigned to the Solid65 element. The failure modes of cracking and crushing are both considered (Referring to the previously stated parameters). (Hemant, et al. 2007 [7]) recommended stress-strain curves for masonry prisms were scaled down with the same trend line to meet the properties of the employed bricks and mortar. Eight masonry prisms were tested in order to evaluate the mechanical properties (masonry characteristic compressive strength f'm), to evaluate the stress-strain curve for masonry constructed from units available in the local Egyptian market. Although many curves can really be found in text books and other references (Hemant, et al. 2007 [7]), Figure 5 depicts the experimental, reference, and adopted curves, with the adopted curve able to anticipate the failure load and load displacement curve with acceptable accuracy.

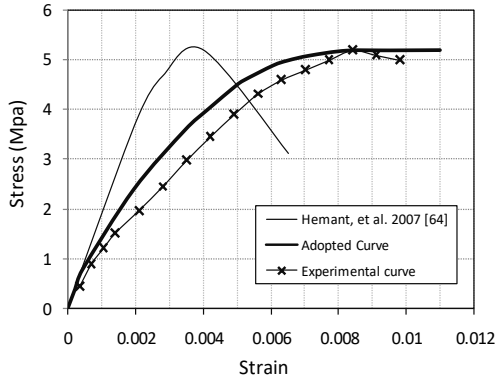

Fig. 5. Compressive stress-strain curves for masonry

2.3 Non-Linear Finite Element for the two case study

As The Non-linear finite element models have three main goals, which are to illustrate the efficiency of the proposed model; verify element and material models; and validate the software program. The Boundary conditions for the models achieved to match the actual conditions in nature as the supporting of footing was achieved by lock the translation X, Y, Z at the appointed locations of the anchors, and selected nodes on bottom edge of footing were locked against vertical and out of plan translation as shown in Figure 6

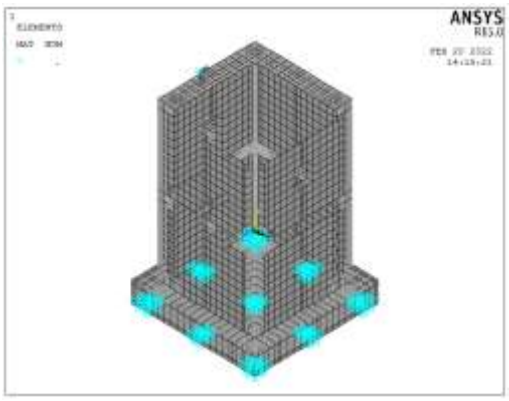

Fig. 6. Boundary conditions and location of horizontal load beam stup

2.3.1 Case Study 1(S-01-FEM)

The case study S-01-FEM was verified using proposed non-linear finite element model. It was loaded laterally by cyclic loading displacement protocol same as shown at Figure 1. Case study S-01-FEM was oriented in such a way that loading was imposed perpendicular to the side of model with door perforations. Typical modeling of the tie-columns, tie-beams, and masonry elements representing the concrete, bricks, and steel rebar is indicated in Figure 7.a to 7.e for models of verification case study S-01-FEM.

Figures 8a to 8i show the cracking patterns obtained from finite element model at cracking load, at maximum load, and finally at ultimate or failure load.

The shear stresses at ultimate load is shown in Figures 8.j to 8.l which clarify that shear stresses in masonry panel have average value of 0.8 Mpa at the diagonal compression strut. Also the shear

stresses at tie-columns reach ranges of 2.75-3.67 MPa which may be classified as accepted maximum shear stresses values for reinforced concrete with compressive strength 26.0 - 27.5 Mpa as mentioned previously.

The mechanical strain at ultimate load is shown in Figure 8.o to 8.r, where the strain in masonry ranging from 0.0075 to 0.058 which may be accepted by the suggested values derived and stated by (Hemant, et al. 2007 [7]) as the proposed ultimate strain equals 0.006. The load-displacement envelope curves from the test and the finite element model are shown in Figure 9.a to 9.e the maximum lateral loads of finite element model are +218 KN and -217 KN for pushing and pulling directions to predict the maximum lateral capacity of model.

The corresponding lateral top displacements at maximum lateral loads from finite element model are +30mm and -28mm respectively for pushing and pulling directions.

The ultimate lateral loads of finite element model are equal +218 KN and -217 KN. The corresponding lateral ultimate displacements at numerical model are +30.0mm and -28.0mm.

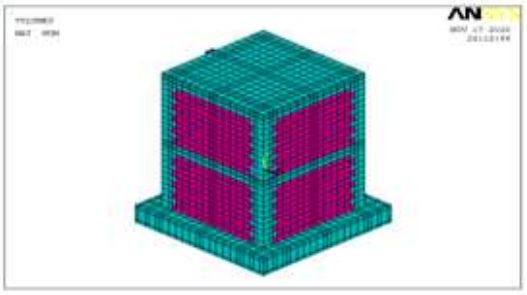

FIG. 7.a Meshing of finite element for specimen

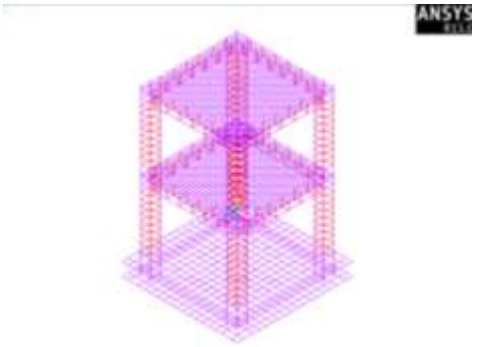

Fig. 7.b Reinforcement of specimens

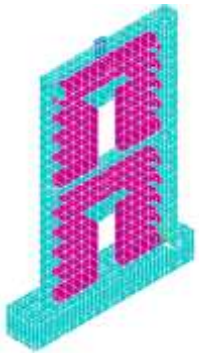

Fig. 7.c**.** Typical meshing (Doors opening)

Fig. 7.d. Typical meshing (Windows Opening)

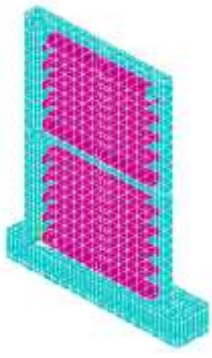

Fig. 7.e. Typical finite element meshing (solid walls).

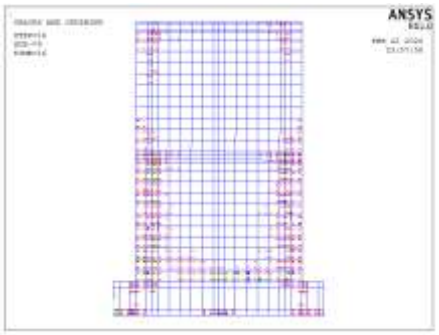

Fig.8.A. cracking pattern at cracking load (at frisk crack) for solid face.

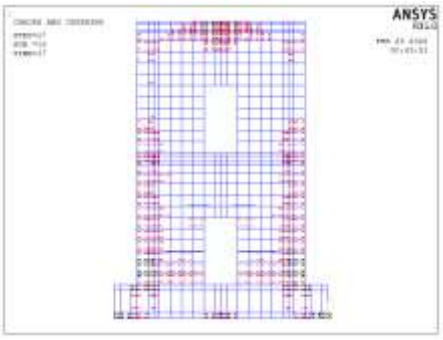

Fig. 8. B. cracking pattern at cracking load (at frisk crack) for face with doors.

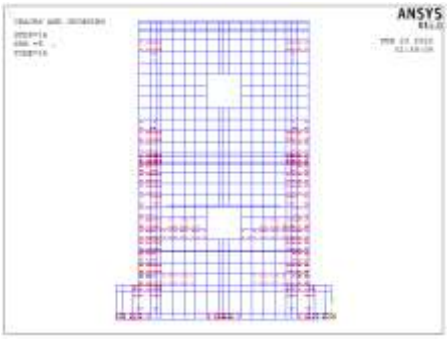

Fig. 8. C. cracking pattern at cracking load (at frisk crack) for face with windows

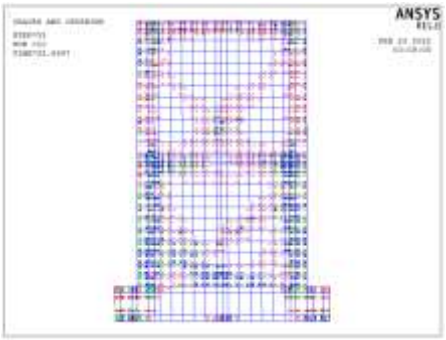

Fig. 8.d. Cracking pattern at cracking load (at ultimate load) for solid face.

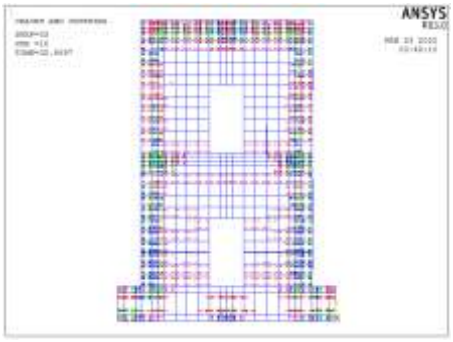

Fig. 8.e. Cracking pattern at cracking load (at ultimate load) for face with doors

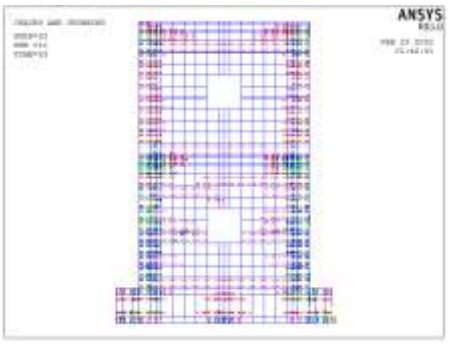

Fig. 8.f. Cracking pattern at cracking load (at ultimate load) for face with windows.

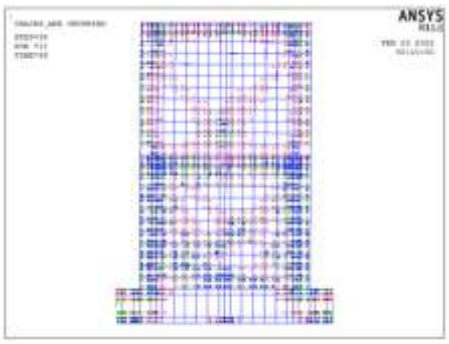

Fig. 8.g. Cracking pattern at cracking load (at failure load) for solid face

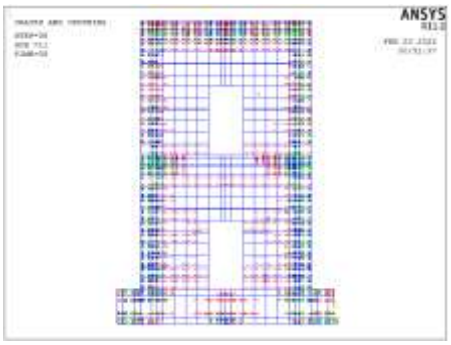

Fig. 8.h. Cracking pattern at cracking load (at failure load) for face with doors.

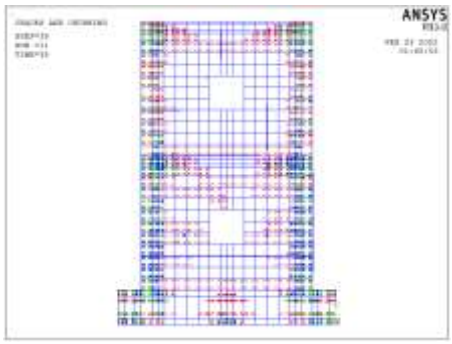

Fig. 8.i. Cracking pattern at cracking load (at failure load) for face with windows.

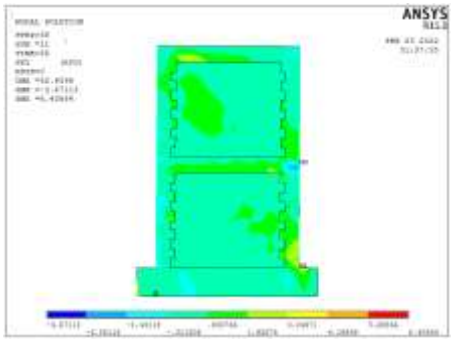

Fig. 8.j. Shear stress (in Mpa) at ultimate load (solid face).

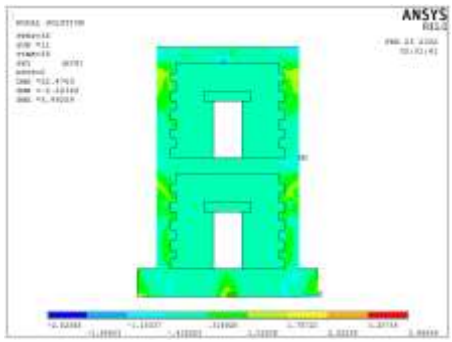

Fig. 8.k Shear stress (in Mpa) at ultimate load (face with doors)

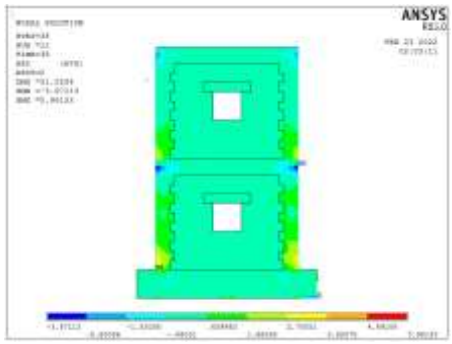

Fig. 8.l. stress (in Mpa) at ultimate load (face with windows).

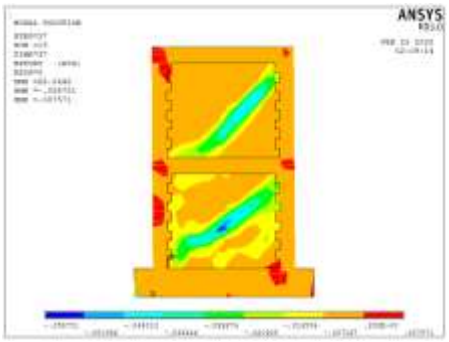

Fig. 8.m. Mechanical strain at ultimate load (solid face) - model at push case.

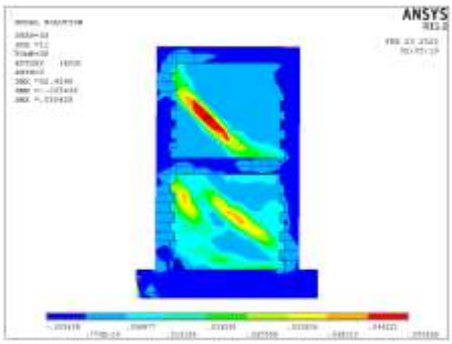

Fig. 8.n. Mechanical strain at ultimate load (solid face) – model at pull case.

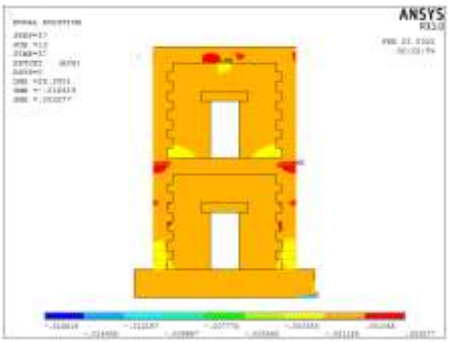

Fig. 8.o. Mechanical strain at ultimate load (face with doors) – model at push case.

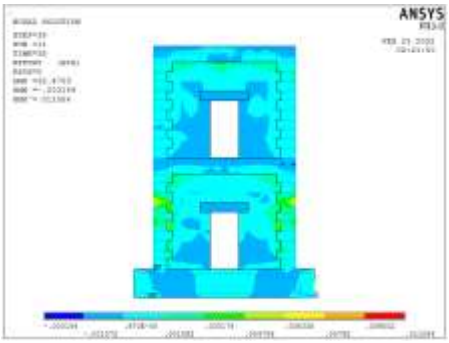

Fig. 8.p Mechanical strain at ultimate load (face with doors) - model at pull case.

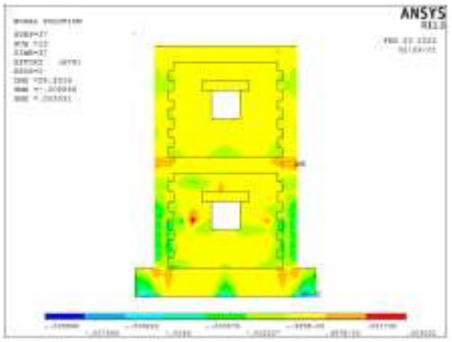

Fig 8.q. Mechanical strain at ultimate load (face with windows) - model at push case.

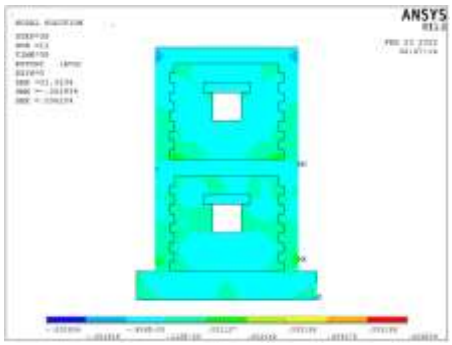

Fig 8.r. Mechanical strain at ultimate load face with windows) - model at pull case

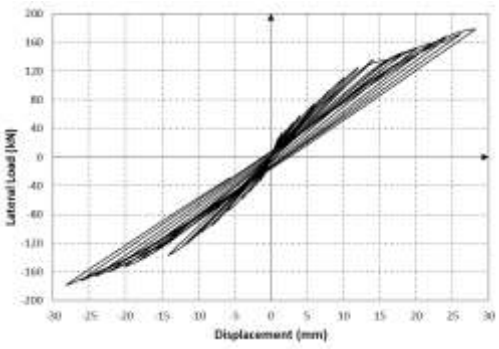

Fig 9.a. Hysteresis loops curves for model (S-01-FEM).

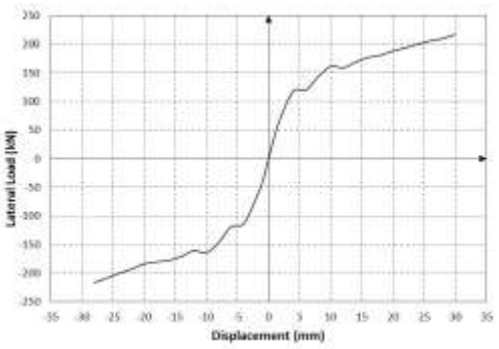

Fig 9.b. Envelope load-displacement curves for model(S-01-FEM).

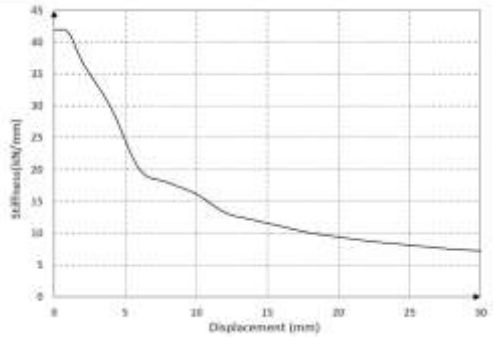

Fig 9.c Stiffness curve for Model (S-01-FEM)

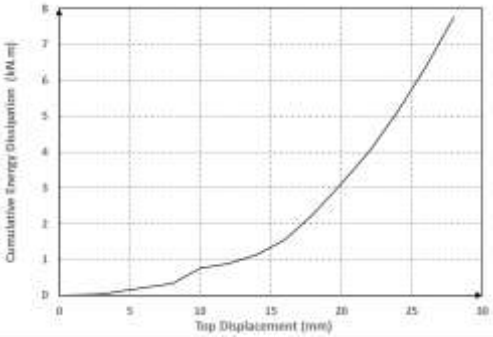

Fig 9.d Cumulative Energy Dissipation (KN.m) Model (S-01-FEM)

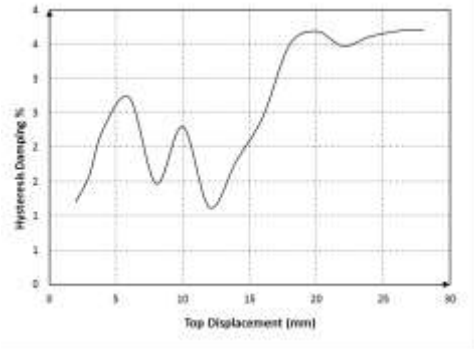

Fig 9.e Hysteresis Damping% for Model (S-01-FEM)

2.3.2 Case Study 1(S-02-FEM)

The case study S-02-FEM was verified using proposed non-linear finite element model. It was loaded laterally by cyclic loading displacement protocol same as shown at Figure 1. Case study S-01-FEM was oriented in such a way that loading was imposed parallel to the side of model with door perforations. Typical modeling of the tie-columns, tie-beams, and masonry elements representing the concrete, bricks, and steel rebar is indicated in Figure 7.a to 7.e for models of verification case study S-02-FEM.

Figures 10.a to 10.i show the cracking patterns obtained from finite element model at cracking load, at maximum load, and finally at ultimate or failure load.

The shear stresses at ultimate load is shown in Figures 10.j to 10.l which clarify that shear stresses in masonry panel have average value of 0.8 Mpa at the diagonal compression strut.

Also the shear stresses at tie-columns reach ranges of 1.22-0.80 MPa which may be classified as accepted maximum shear stresses values for reinforced concrete with average compressive strength 26.0 - 27.5 Mpa.

The mechanical strain at ultimate load is shown in Figure 10.o to 10.r, where the strain in masonry ranging from 0.0075 to 0.058 which may be accepted by the suggested values derived and stated by (Hemant, et al. 2007 [**7**]) as the proposed ultimate strain equals 0.027.

The load- displacement envelope curves from the test and the finite element model are shown in Figure 11.a to 11.e the maximum lateral loads of finite element model are +203 KN and -208 KN for pushing and pulling directions with compared to +169 KN and -154 KN obtained from experimental test with good agreement level to predict the maximum lateral capacity of model.

The corresponding lateral top displacements at maximum lateral loads from finite element model are +38.0mm and -44.0mm respectively for pushing and pulling directions, so good agreement can be achieved by finite element modeling to predict the corresponding deformations at maximum lateral load capacities.

The ultimate lateral loads of finite element model are equal +203KN and -208 KN. The corresponding lateral ultimate displacements at numerical model are +48.0mm and -48.0mm.Results from the finite element model S-02-FEM have showed that the developed model is capable, with sufficient degree of accuracy.

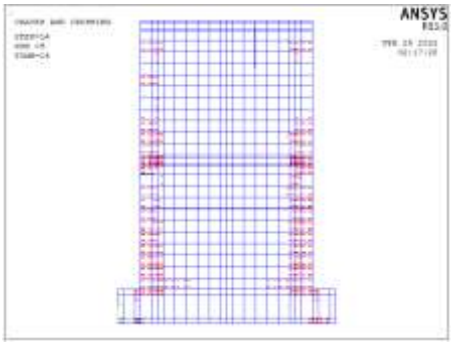

Fig 10.a. cracking pattern at cracking load (at frisk crack) for solid face – model (S-02-FEM)

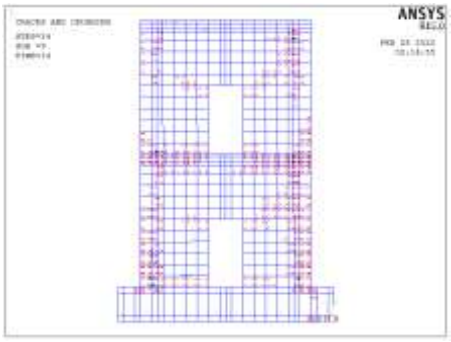

Fig 10.b. Cracking pattern at cracking load (at frisk crack) for face with doors – model(S-02-FEM).

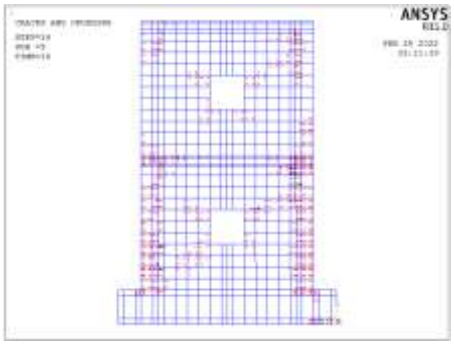

Fig 10.c. Cracking pattern at cracking load (at frisk crack) for face with windows - model (S-02-FEM).

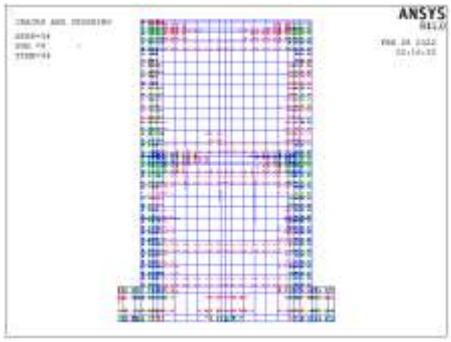

Fig 10.d. Cracking pattern at cracking load (at ultimate load) for solid face - model (S-02-FEM).

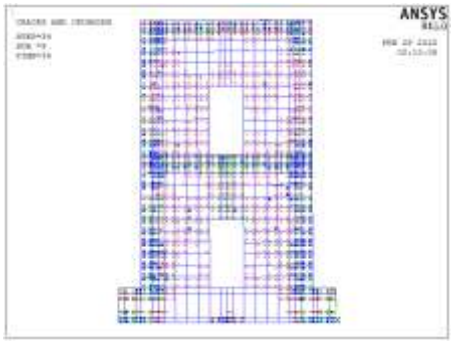

Fig 10.e. Cracking pattern at cracking load (at ultimate load) for face with doors - (S-02-FEM).

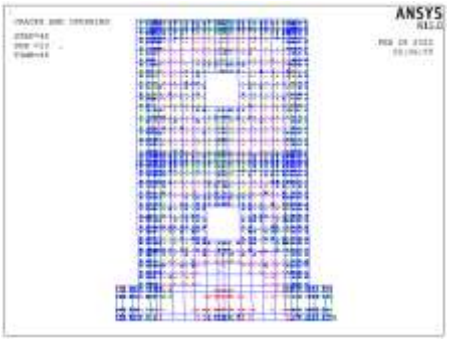

Fig 10.i. Cracking pattern at cracking load (at failure load) for face with windows – (S-02-FEM).

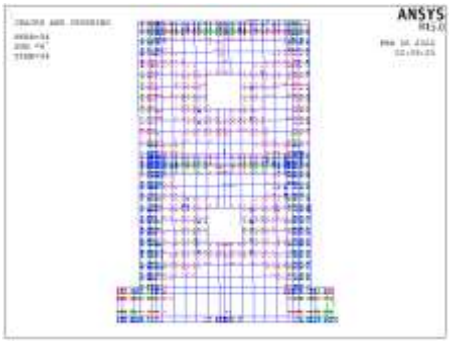

Fig 10.f. Cracking pattern at cracking load (at ultimate load) for face with windows - (S-02-FEM)

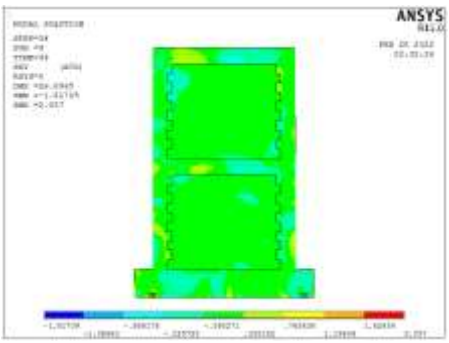

Fig 10.j. Shear stress (in Mpa) at ultimate load (solid face) - model (S-02-FEM).

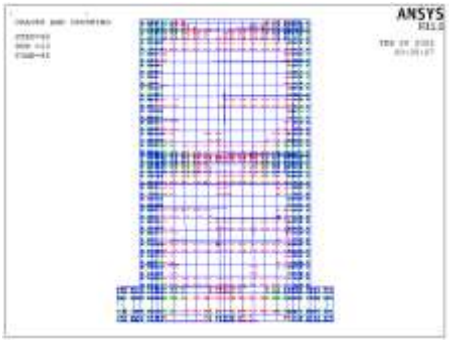

Fig 10.g. Cracking pattern at cracking load (at failure load) for solid face - model (S-02-FEM)

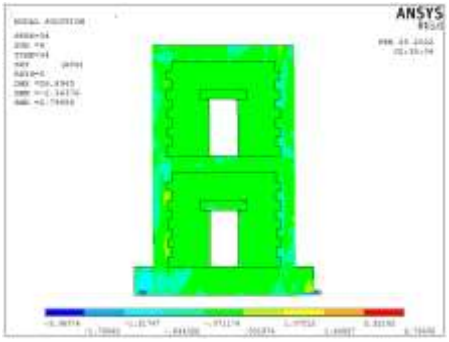

Fig 10.k Shear stress (in Mpa) at ultimate load (face with doors) - model (S-02-FEM)

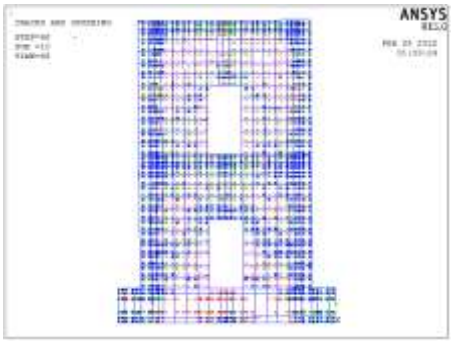

Fig 10.h. Cracking pattern at cracking load (at failure load) for face with doors – (S-02-FEM).

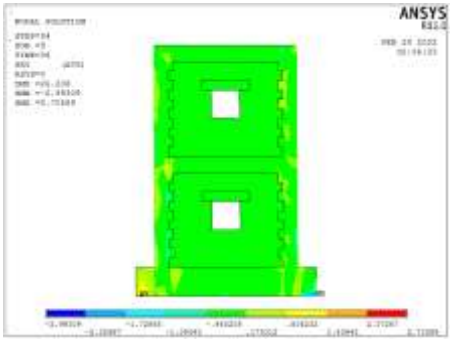

Fig 10.l. stress XY (in Mpa) at ultimate load (face with windows) - model (S-02-FEM).

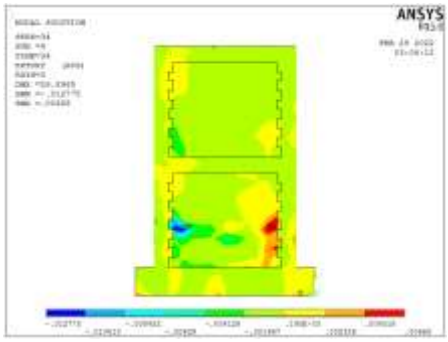

Fig 10.m. Mechanical strain at ultimate load (solid face) - model (S-02-FEM) at push case.

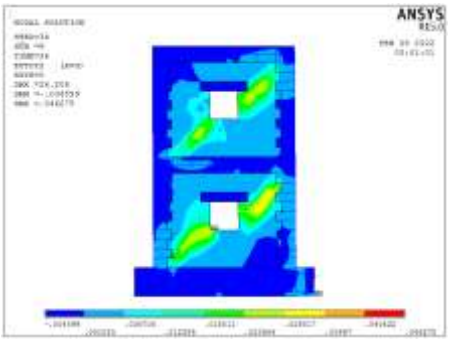

Fig 10.q. Mechanical strain at ultimate load (face with windows) – (S-02-FEM) at push case.

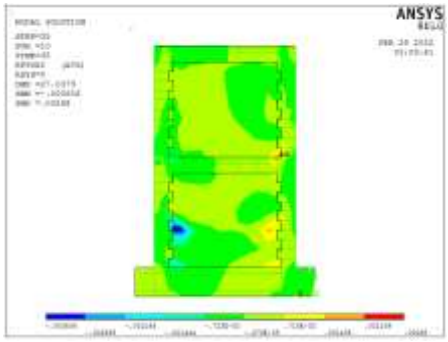

Fig 10.n. Mechanical strain at ultimate load (solid face) – model (S-02-FEM) at pull case.

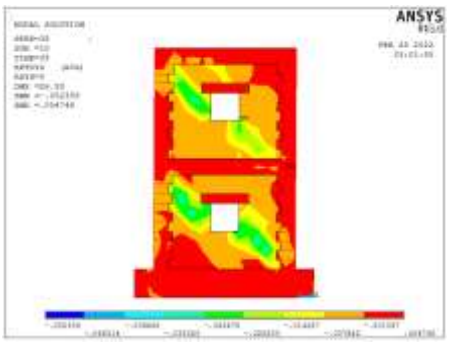

Fig 10.r. Mechanical strain at ultimate load face with windows) - model (S-02-FEM) at pull case.

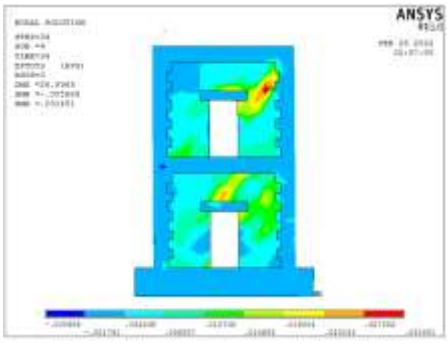

Fig 10.o. Mechanical strain at ultimate load (face with doors) – model (S-02-FEM) at push case

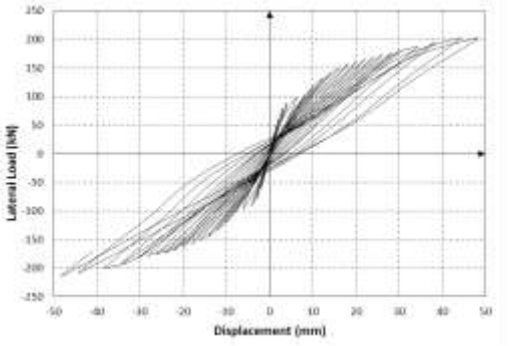

Fig 11.a. Hysteresis loops curves for- model (S-02-FEM).

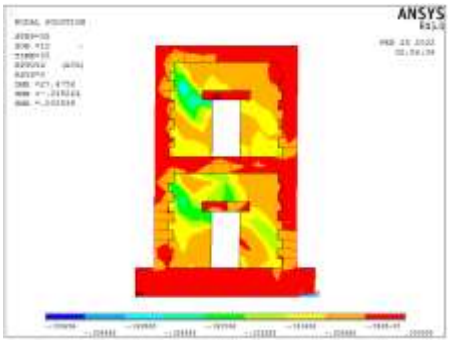

Fig 10.p Mechanical strain at ultimate load (face with doors) - model (S-02-FEM) at pull case.

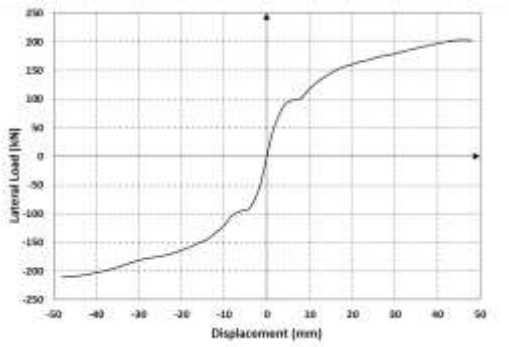

Fig 11.b. Envelope load-displacement curves for - model (S-02-FEM).

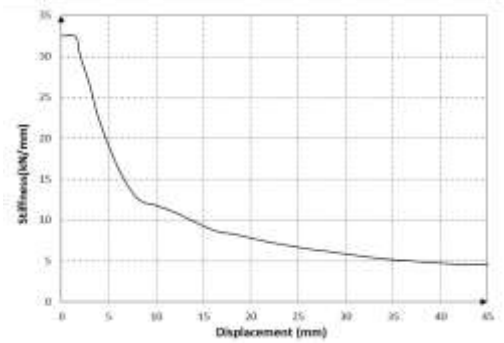

Fig 11.c Stiffness curve for – (S-02-FEM)

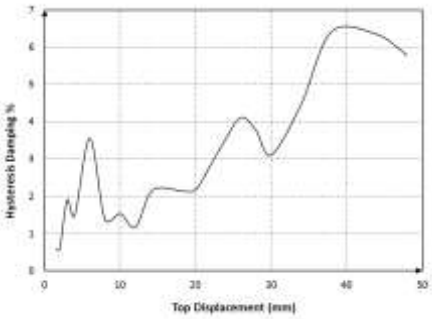

Fig 11.e Hysteresis Damping% for – (S-02-FEM)

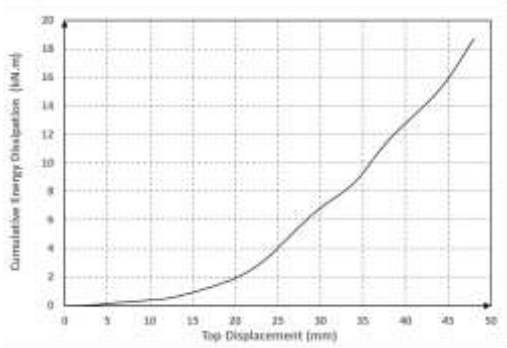

Fig 11.d Cumulative Energy Dissipation (KN.m) - model (S-02-FEM)

3.0 Analytical Study of In-plan and out-of-plan performance of Confined Masonry Building.

The goal of this section is to create 3D finite element models to study of In-plan and out-of-plan performance of Confined Masonry Building that can capture the essential response aspects of failure mode shapes and crack patterns for each specimen and comparing them with case study no.1 (S-01-FEM) and case study no.1 (S-02-FEM).Seven models with a 0.40-scale were created with two stories. The models consisted of a clay masonry panel, eight confining columns, eight tie beams and two slabs. The models were analyzed under a lateral cyclic loading with displacement-controlled loading protocol up to failure as mentioned in chapter 6.

Table. 1 summarizes the analytical models.

Model ID.	***Front elevation***	***Back elevation***	***Right side view***	***Left side view***	***Long. RFT.***	***Trans RFT.***
S-01-FEM	*Solid walls*	*Solid walls*	*Walls with doors*	*Walls with windows*	*T6@20cm*	*4T10*
S-0-FEM-E	*Empty*	*Empty*	*Empty*	*Empty*	*T6@20cm*	*4T10*
S-01-FEM-M	*Solid walls*	*Solid walls*	*Walls with doors*	*Walls with windows*	------	------
S-01-FEM-I	*Solid walls*	*Solid walls*	*Empty*	*Empty*	*T6@20cm*	*4T10*
S-01-FEM-O	*Empty*	*Empty*	*Walls with doors*	*Walls with windows*	*T6@20cm*	*4T10*
S-02-FEM	*Walls with doors*	*Walls with windows*	*Solid walls*	*Solid walls*	*T6@20cm*	*4T10*
S-02-FEM-M	*Walls with doors*	*Walls with windows*	*Solid walls*	*Solid walls*	------	------
S-02-FEM-I	*Walls with doors*	*Walls with windows*	*Empty*	*Empty*	*T6@20cm*	*4T10*
S-02-FEM-O	*Empty*	*Empty*	*Solid walls*	*Solid walls*	*T6@20cm*	*4T10*

3.1 Analytical model (S-0-FEM-E)

The purpose of model (S-0-FEM-E) is to evaluate the concrete frame from its singular of lateral horizontal loads. Model (S-0-FEM-E) consists of two story with no masonry walls. Typical modeling of the tie-columns, tie-beams, and slabs elements representing the concrete and steel rebar is indicated in Figure 12.

Figures 13.a to 13.c show the cracking patterns obtained from finite element model at failure load. The figures show that the failure of this model is flexural failure in the columns act as portal frame.

The shear stresses at failure load is shown in Figure 13.d which clarify that shear stresses in concrete tie-columns have average value at tie-columns reach ranges of 1.34-10.34 MPa. The mechanical strain at failure load is shown in Figure 13.e, where the strain in ranging from 0.0296 to 0.00864.

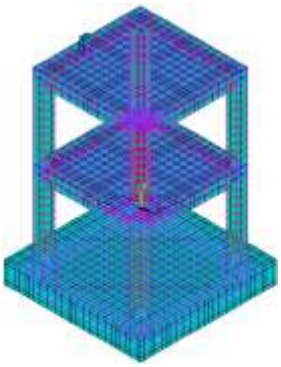

Fig 12. Finite element model characterization and meshing for model (S-0-FEM-E).

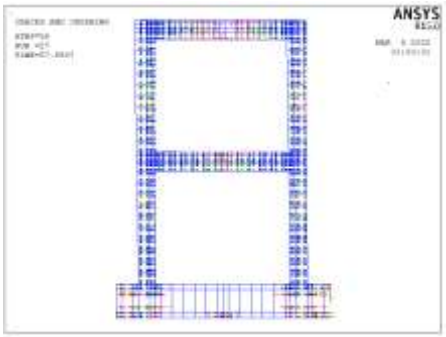

Fig 13.a. Cracking pattern at failure load (elevation) –Model (S-0-FEM-E).

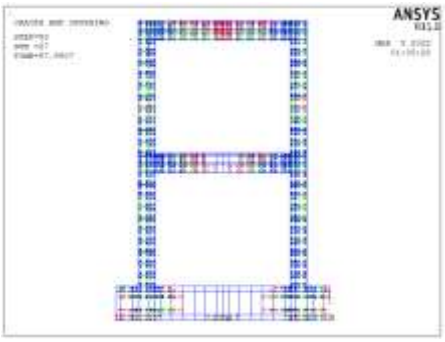

Fig 13.b. Cracking pattern at failure load (front elevation) –Model (S-0-FEM-E).

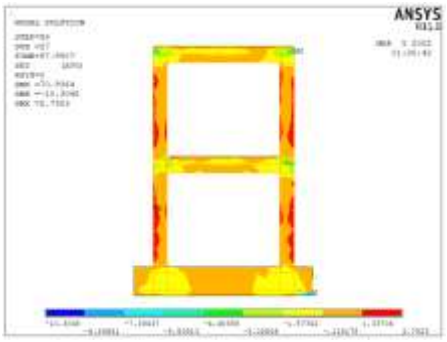

Fig 13.d. Shear stress (in Mpa) at failure load – Model (S-0-FEM-E).

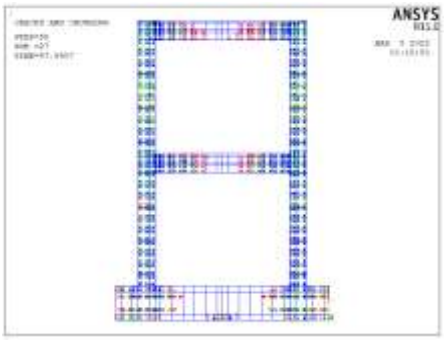

Fig 13.c. Cracking pattern at failure load (left/right side view) – Model (S-0-FEM-E).

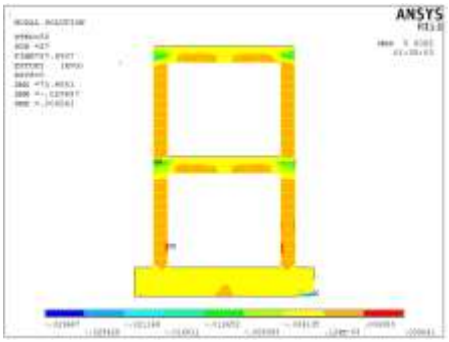

Fig 13.e. Mechanical strain at failure load - Model (S-0-FEM-E)

3.2 Analytical model (S-0-FEM-E

The purpose of model (S-01-FEM-M) is to evaluate the effect of the solid masonry walls only to resist the lateral horizontal loads. Model (S-01-FEM-M) consists of two story with masonry walls only. The model consists of two storey with two slabs surrounding with tie beams, where the columns in this model not excited. The front and back elevation of model is solid wall towards parallel to the horizontal load, the left-side view of the model is masonry wall with two windows where the right-side view of the model is masonry wall with two doors towards perpendicular to the horizontal load. Typical modeling of the slabs, tie-beams, and masonry elements representing the concrete, bricks, and steel rebar is indicated in Figure 14.Figures 15.a to 15.c show the cracking patterns obtained from finite element model at ultimate or failure load. The figures of crack patterns show that the failure of this model is shear failure happened in the bottom of all masonry walls as shown.The shear stresses at ultimate load are shown in Figures 15.d to 15.f which clarify that shear stresses in masonry panel have average value of 0.29Mpa. The mechanical strain at ultimate load is shown in Figure 7.14g, where the strain in masonry ranging from 0.013 to 0.043.

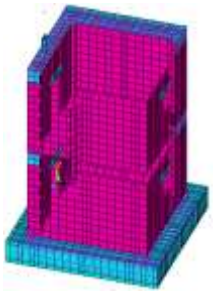

Fig 14. Finite element model characterization and meshing for model (S-01-FEM-M).

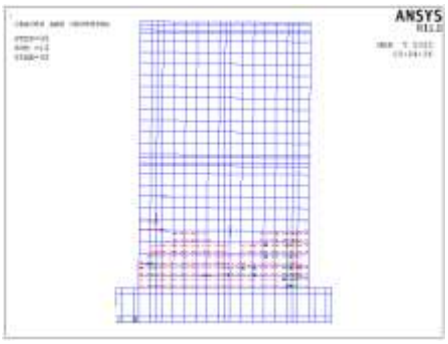

Fig 15.a. Cracking pattern at failure load (front/back elevation) –Model (S-01-FEM-M).

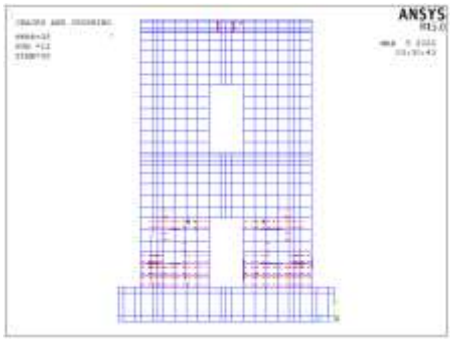

Fig 15.b. Cracking pattern at failure load (left side view) –Model (S-01-FEM-M).

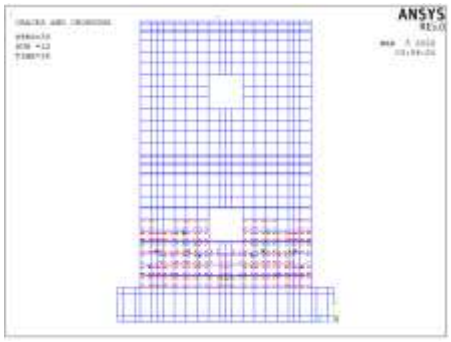

Fig 15.c. Cracking pattern at failure load (right side view) – Model (S-01-FEM-M).

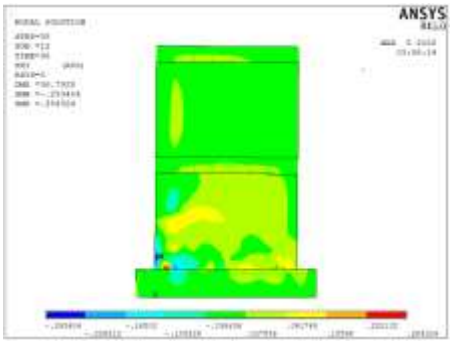

Fig 15.d. Shear stress (in Mpa) at failure load - (front/back elevation) –Model (S-01-FEM-M).

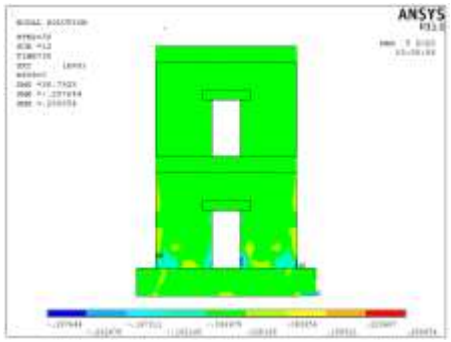

Fig 15.e. Shear stress (in Mpa) at failure load - (left side view) – Model (S-01-FEM-M)

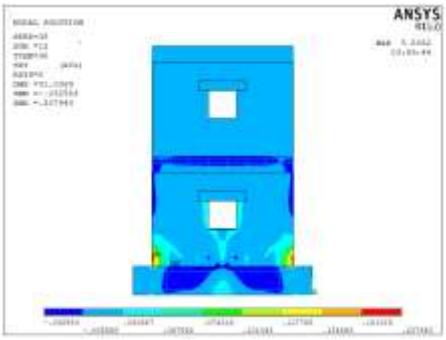

Fig 15.f. Shear stress (in Mpa) at failure load - (right side view) –Model (S-01-FEM-M).

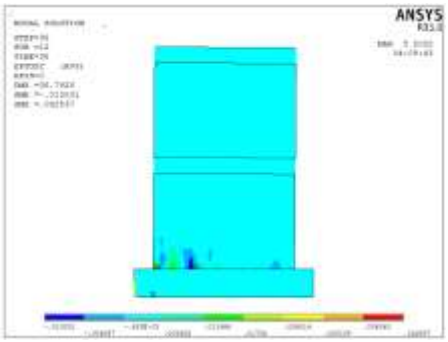

Fig 15.g. Mechanical strain at failure load - (front/back elevation) – Model (S-01-FEM-M).

3.3 Analytical model (S-01-FEM-I)

The purpose of model (S-01-FEM-I) is to evaluate the effect of the confined solid masonry walls in plan of loading without any walls in direction of out-plan of model towards to the lateral horizontal loads. Model (S-01-FEM-I) consists of two story with two masonry walls only. The model consists of two storey with two slabs surrounding with tie beams, and tie-columns in this model. The front and back elevation of model is consisted of solid wall parallel towards to the horizontal lateral load, where the left and right-side view of the model are empty from wall towards to perpendicular to the horizontal load. Typical modeling of the tie-columns, slabs, tie-beams and masonry elements representing the concrete, bricks, and steel rebar is indicated in Figure 16.Figures 17.a to 17.b show the cracking patterns obtained from finite element model at ultimate or failure load. The failure of the model may be classified as combined flexural cracking at tie-columns and diagonal shear crack propagated in confined masonry elements as shown in figures. The shear stresses at ultimate load are shown in Figures 17.c to 17.d, which clarify that shear stresses in masonry panel have average value of 0.8Mpa at the diagonal compression strut. Also, the shear stresses at tie-columns reach ranges of 3.90-4.30MPa.The mechanical strain at ultimate load is shown in Figure 17.e, where the strain in masonry ranging from 0.0074 to 0.054.

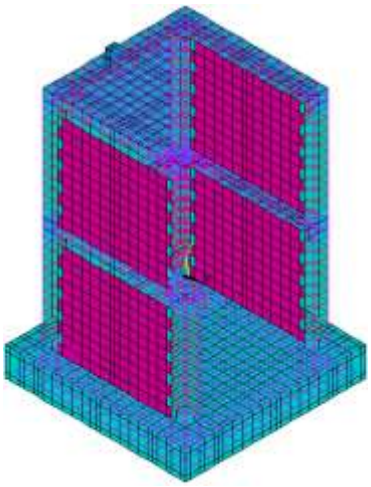

Fig 16. Finite element model characterization and meshing for model (S-01-FEM-I).

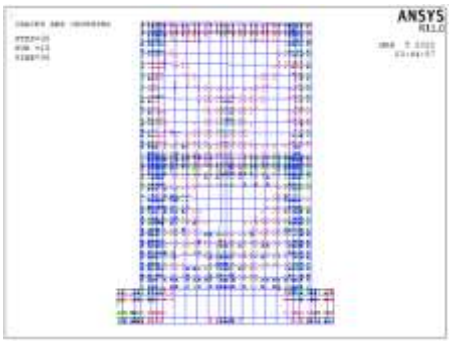

Fig 17.a. Cracking pattern at failure load (front/back elevation) –Model (S-01-FEM-I).

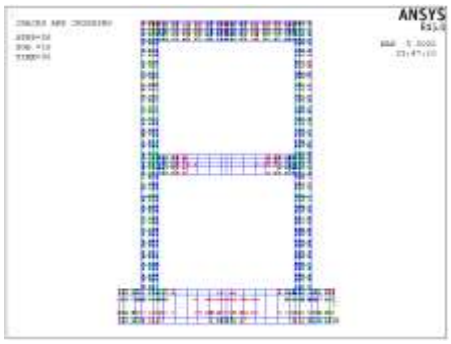

Fig 17.b. Cracking pattern at failure load (left/right side view) –Model (S-01-FEM-I)

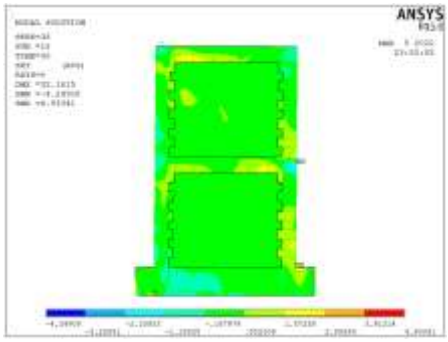

Fig 17.c. Shear stress (in Mpa) at failure load - (front/back elevation) – Model (S-01-FEM-I).

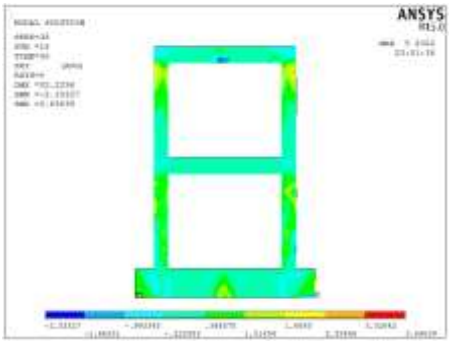

Fig 17.d. Shear stress (in Mpa) at failure load - (left/right side view) – Model (S-01-FEM-I).

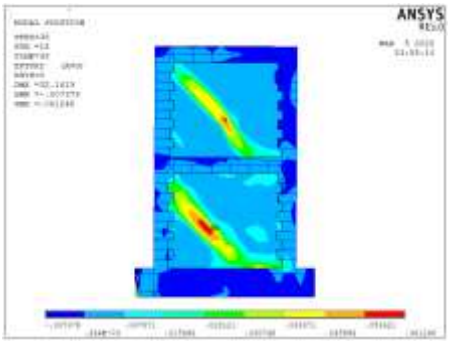

Fig 17.e. Mechanical strain at failure load - (front/back elevation) – Model (S-01-FEM-I).

3.4 Analytical model (S-01-FEM-O)

The purpose of model (S-01-FEM-O) is to evaluate the effect of the confined masonry walls with openings (doors and windows) in out-plan of loading without any wall in the in-plan of model on the lateral horizontal loads. Model (S-01-FEM-O) consists of two story with two masonry walls only, two slabs surrounding with tie beams and tie-columns in this model. the front and back elevation of model is empty from wall parallel to the horizontal load, where the left consists of wall with opening (two doors) where right-side view consists of wall with opening (two windows) perpendicular to the horizontal load. Typical modeling of the tie-columns, slabs, tie-beams and masonry elements representing the concrete, bricks, and steel rebar is indicated in Figure 18.

Figures 19.a to 19.c show the cracking patterns obtained from finite element model at ultimate or failure load. The figures of cracking patterns show that the failure of this model is flexural failure in the columns act as portal frame incorporating with out-plan walls. The shear stresses at ultimate load are shown in Figures 19.d to 19.f, which clarify that shear stresses in masonry panel have average value of 0.8Mpa. Also, the shear stresses at tie-columns reach ranges of 3.17-8.8MPa.The mechanical strain at ultimate load is shown in Figure 7.20f, where the strain in masonry ranging from 0.033 to 0.075.

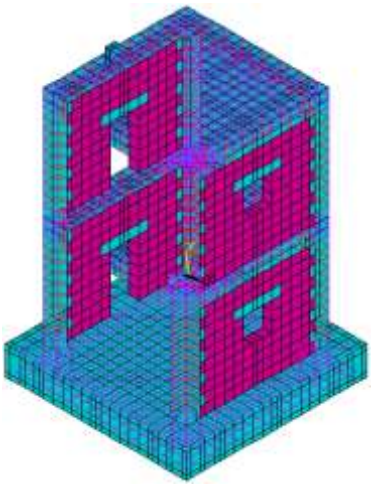

Fig 18. Finite element model characterization and meshing for model (S-01-FEM-O).

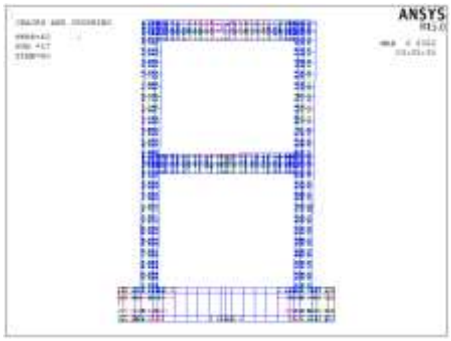

Fig 19.a. Cracking pattern at failure load (front/back elevation) –Model (S-01-FEM-O).

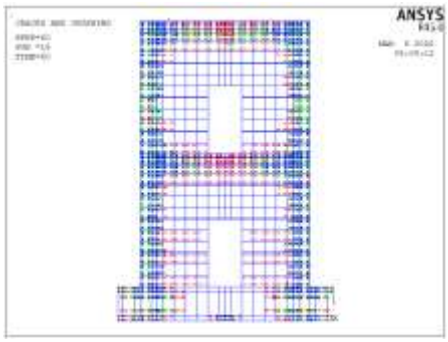

Fig 19.b. Cracking pattern at failure load (left side view) –Model (S-01-FEM-O).

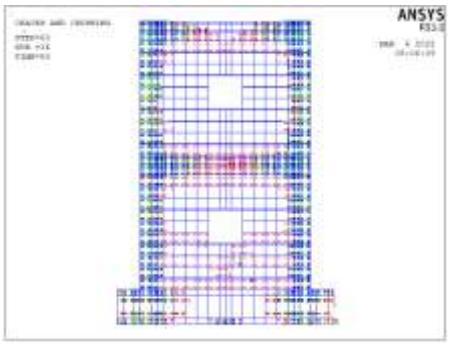

Fig 19.c. Cracking pattern at failure load (right side view) Model (S-01-FEM-O).

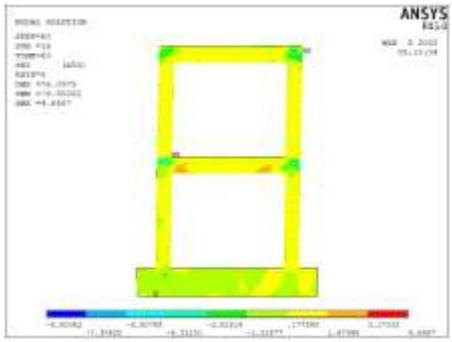

Fig 19.d. Shear stress (in Mpa) at failure load - (front/back elevation) – Model (S-01-FEM-O).

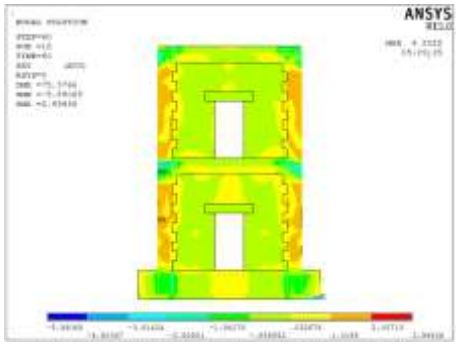

Fig 19.e. Shear stress (in Mpa) at failure load - (left side view) – Model (S-01-FEM-O)

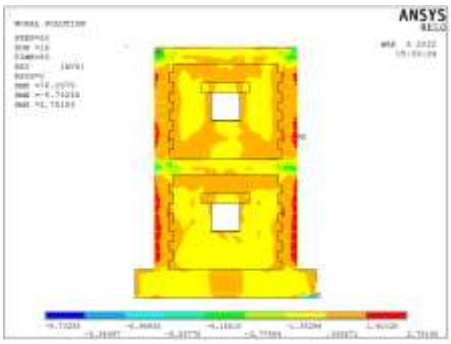

Fig 19.f. Shear stress (in Mpa) at failure load - (right side view) – Model (S-01-FEM-O).

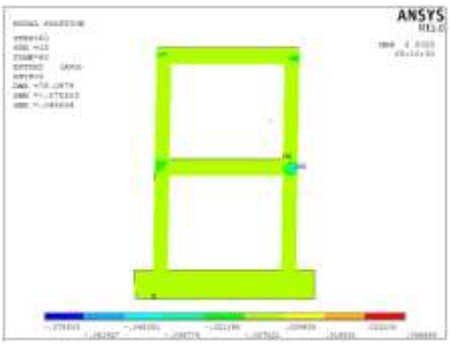

Fig 19.g. Mechanical strain at failure load - (front/back elevation) – MODEL (S-01-FEM-O).

3.5 Analytical model (S-02-FEM-M)

The purpose of model (S-02-FEM-M) is to evaluate the effect of the confined masonry walls only on the direction of lateral horizontal loads. Model (S-02-FEM-M) consists of two story with masonry walls only. The model consists of two storey with two slabs surrounding with tie beams, where the columns in this model not excited. the front elevation of model consists of wall with opening (two doors) parallel to the horizontal load and the back elevation of model consists of wall with opening (two windows) where the left and right-side view of the model consist of two solid walls perpendicular to the direction of lateral horizontal load.

Typical modeling of the slabs, tie-beams, and masonry elements representing the concrete, bricks, and steel rebar is indicated in Figure 20.

Figures 21.a to 21.c show the cracking patterns obtained from finite element model at ultimate or failure load. The figures of crack patterns show that the failure of this model is shear failure happened in the bottom of all masonry walls as shown.

The shear stresses at ultimate load are shown in Figures 21.d to 21.f which clarify that shear stresses in masonry panel have average value of 0.8Mpa.

The mechanical strain at ultimate load is shown in Figures 21.g, h where the strain in masonry ranging from 0.005 to 0.02.

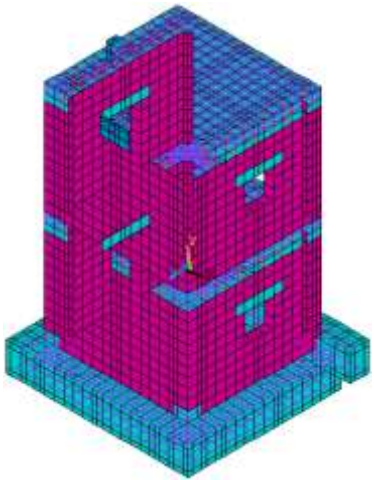

Fig 20. Finite element model characterization and meshing for model (S-02-FEM-M).

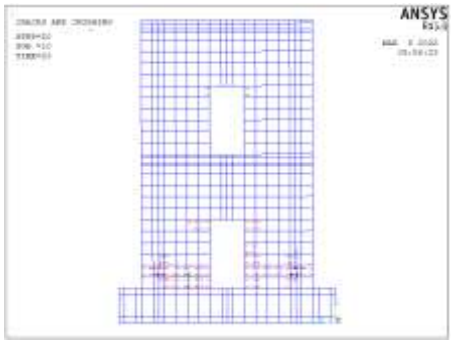

Fig 21.a Cracking pattern at failure load (front elevation) –Model (S-02-FEM-M).

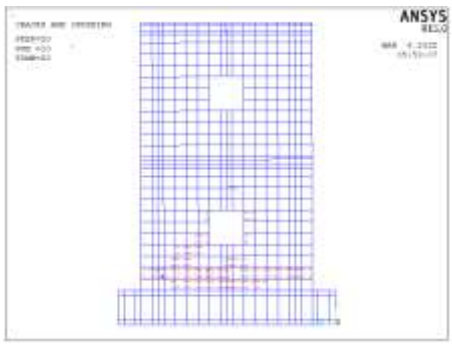

Fig 21.b. Cracking pattern at failure load (back elevation) –Model (S-02-FEM-M).

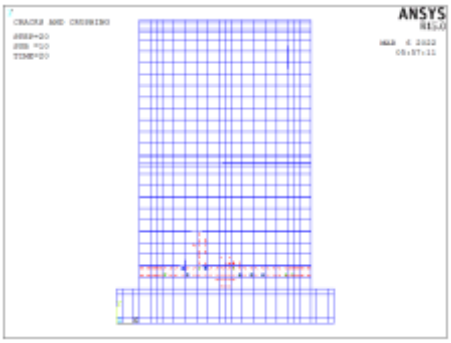

Figure 21.c. Cracking pattern at failure load (left/right side view) –Model (S-02-FEM-M).

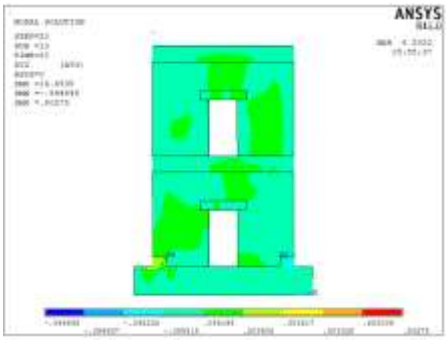

Fig 21.d. Shear stress (in Mpa) at failure load - (front elevation) – Model (S-02-FEM-M).

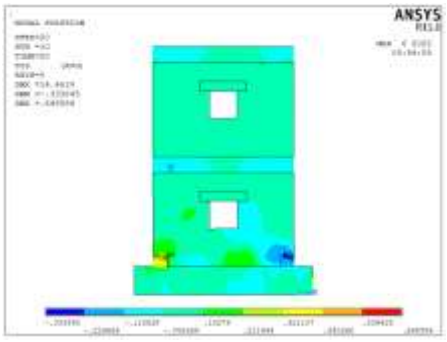

Fig 21.e. Shear stress (in Mpa) at failure load - (back elevation) – Model (S-02-FEM-M)

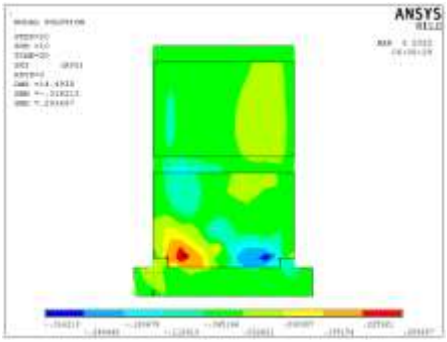

Fig 21.f. Shear stress (in Mpa) at failure load - (left/right side view) – Model (S-02-FEM-M).

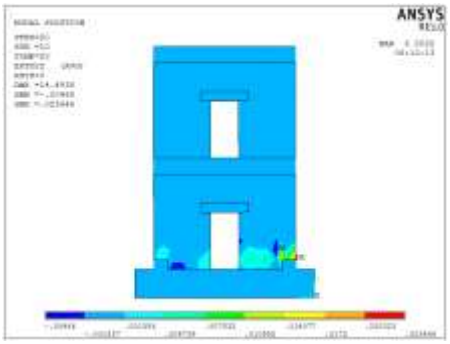

Fig 21.g. Mechanical strain at failure load - (front elevation) Model (S-02-FEM-M).

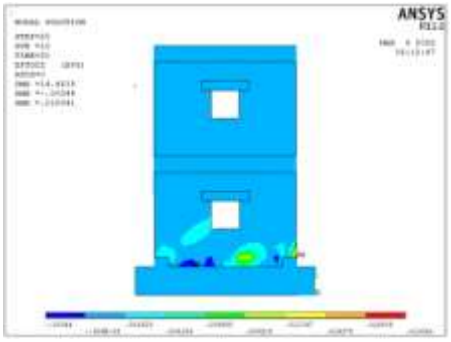

Fig 21.h. Mechanical strain at failure load - (back elevation) – Model (S-02-FEM-M).

3.6 Analytical model (S-02-FEM-I)

The purpose of model (S-02-FEM-I) is to evaluate the effect of the confined solid masonry walls in the direction of in- plan of loading without any wall in the out-plan of model to resist the lateral horizontal loads. Model (S-02-FEM-I) consists of two story with two masonry walls only. The model consists of two story with two slabs surrounding with tie beams, and tie-columns in this model. The front elevation of model is consisted of wall with opening (two doors) where the back elevation of model is consisted of wall with opening (two windows)parallel to the horizontal load, where the left and right-side view of the model are empty from wall perpendicular to the horizontal lateral load. Typical modeling of the tie-columns, slabs, tie-beams and masonry elements representing the concrete, bricks, and steel rebar is indicated in Figure 22.

Figures 23.a to 23.b show the cracking patterns obtained from finite element model at ultimate or failure load. The failure of the model may be classified as combined flexural cracking at tie-columns and diagonal shear crack propagated in confined masonry elements as shown in figures.

The shear stresses at ultimate load are shown in Figures 23.c to 23.d which clarify that shear stresses in masonry panel have average value of 0.8Mpa at the diagonal compression strut. Also, the shear stresses at tie-columns reach ranges of 4.95-5.5MPa. The mechanical strain at ultimate load is shown in Figure 23.e, f, where the strain in masonry ranging from 0.02 to 0.08.

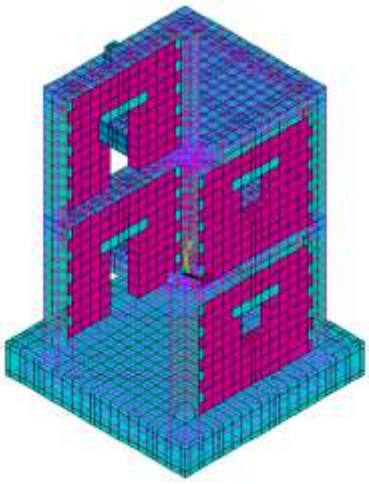

Fig 22. Finite element model characterization and meshing for model (S-02-FEM-I).

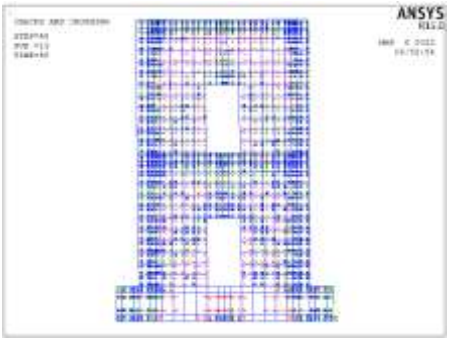

Fig 23.a. Cracking pattern at failure load (front elevation) –Model (S-02-FEM-I).

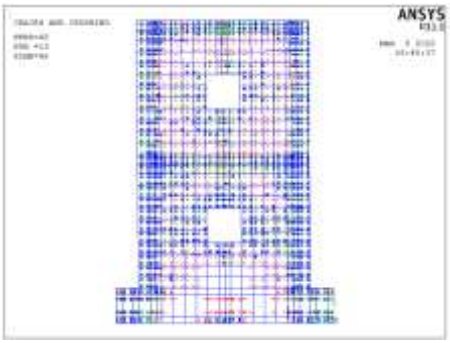

Fig 23.b. Cracking pattern at failure load (back elevation) –Model (S-02-FEM-I).

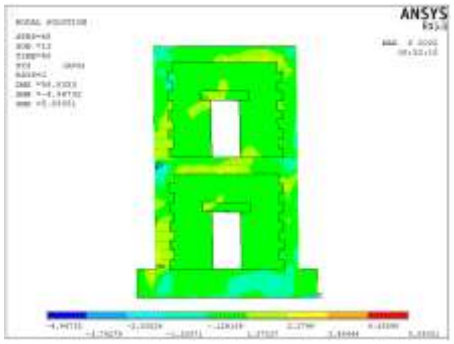

Fig 23.c. Shear stress (in Mpa) at failure load - (front elevation) – Model (S-02-FEM-I).

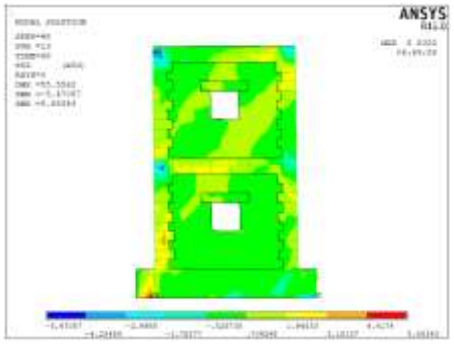

Fig 23.d. Shear stress (in Mpa) at failure load - (back elevation) – Model (S-02-FEM-I).

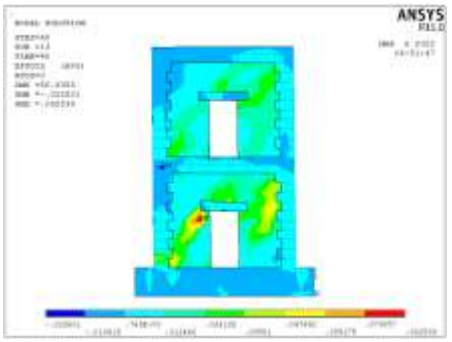

Fig 23.e Mechanical strain at failure load - (front elevation) – Model (S-02-FEM-I).

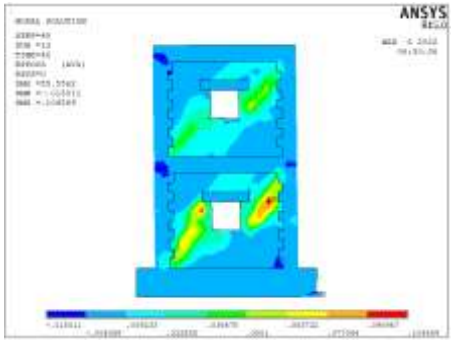

Fig 23.f. Mechanical strain at failure load - (back elevation) –model (S-02-FEM-I).

3.7 Analytical model (S-02-FEM-O)

The purpose of model (S-02-FEM-O) is to evaluate the effect of the confined solid masonry walls in out-plan of loading without any masonry wall in the in-plan of model to resist the lateral horizontal loads. Model (S-02-FEM-O) consists of two story with two masonry walls only, two slabs surrounding with tie beams and tie-columns in this model. The front and back elevation of model is empty from wall parallel to the direction of horizontal lateral load, where the left and right-side view consists of solid walls perpendicular to the direction horizontal lateral load which empty from walls.

Typical modeling of the tie-columns, slabs, tie-beams and masonry elements representing the concrete, bricks, and steel rebar is indicated in Figure 24.

Figures 25.a to 25.b show the cracking patterns obtained from finite element model at ultimate or failure load. The failure type of this model shows flexural failure with incorporating with the solid masonry walls in out-plan of the model.

The shear stresses at ultimate load are shown in Figures 25.c to 25.d which clarify that shear stresses in masonry panel have average value of 0.09Mpa at the diagonal compression strut. Also, the shear stresses at tie-columns reach ranges of 5.5-6.4MPa. The mechanical strain at ultimate load is shown in Figure 25.e, f, where the strain in ranging from 0.01 to 0.045**.**

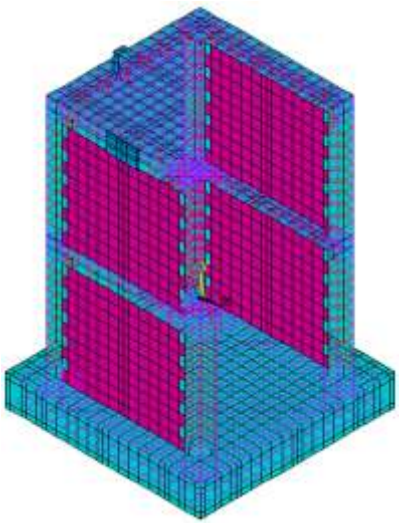

Fig 24. Finite element model characterization and meshing for model (S-02-FEM-O).

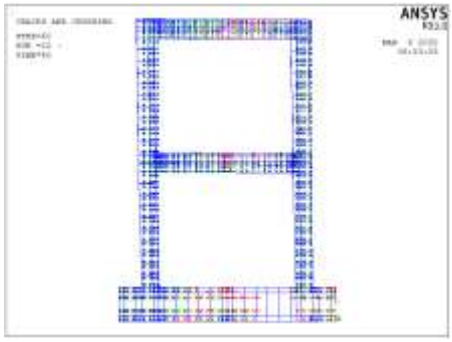

Fig 25.a. Cracking pattern at failure load (front/back elevation) –Model (S-02-FEM-O).

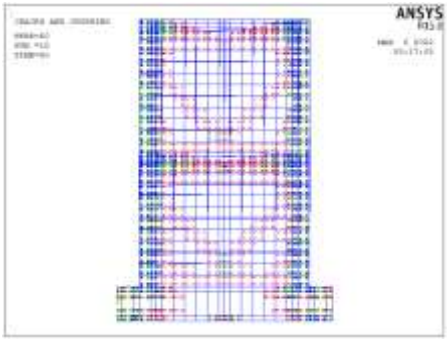

Fig 25.b. Cracking pattern at failure load (left/right side view) –Model (S-02-FEM-O).

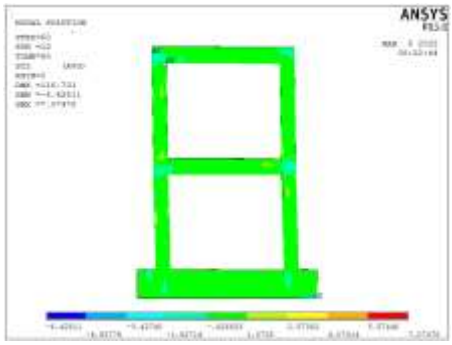

Fig 25.c. Shear stress (in Mpa) at failure load - (front/back elevation) –Model (S-02-FEM-O).

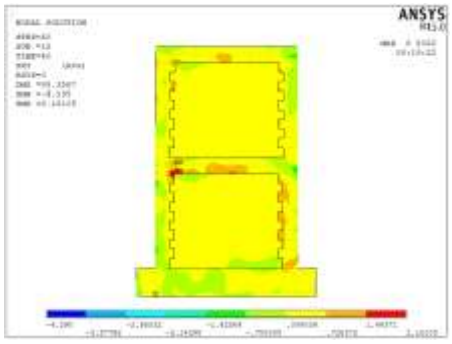

Fig 25.d. Shear stress (in Mpa) at failure load - (left/right side view) – Model (S-02-FEM-O).

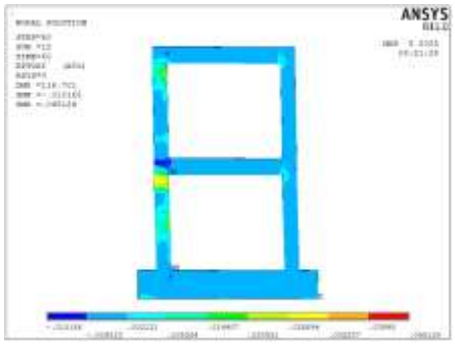

Fig 25.e Mechanical strain at failure load - (front/back elevation) – Model (S-02-FEM-O)

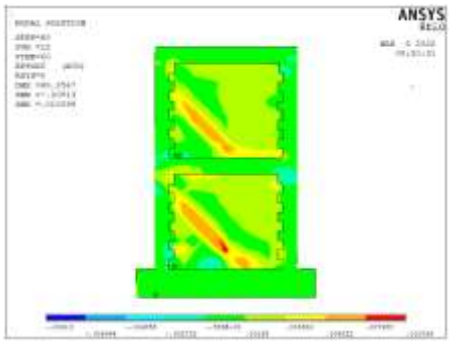

Fig 25.f Mechanical strain at failure load - (left/right side view) – Model (S-02-FEM-O).

4.0 THE EFFECT OF IN-PLAN AND OUT-OF-PLAN WALLS ON PERFORMANCE OF CONFINED MASONRY BUILDING

The purpose of this study is to evaluate the effect of out-plan walls and in-plan walls on the models of both case studies (S-0-1-FEM) and (S-02-FEM), also to study how much elements participate in the model such as the existing of tie-columns in the model, when the model empty from any walls.

The following study show the effect of each item.

4.1 The of effect of In-plan and out-of-plan performance in case study (S-01-FEM)

4.1.1 Effect of absence of masonry walls

The following table 2 show the effect of absence of masonry walls on the model, in case of the absence of masonry walls in the model, the maximum load was decreased by 53%, 47% for push and pull respectively ,the maximum displacement increased by 130%, 154% for push and pull respectively the stiffness reduced by 77%, the Cumulative Energy Dissipation controlled by maximum displacement of control model(S-01-FEM) decreased by 82.5% and the Hysteresis Damping % controlled by

maximum displacement of control model(S-01-FEM) decreased by 25% .This study demonstrated the importance of masonry walls for improvement of confined masonry building to resist the lateral loads and it's considered the main important structural element in design of confined masonry building.

Table 2 –comparison of test results for model (S-01-FEM) and (S-01-FEM-E) in case of absence of masonry walls

		S-01-FEM	*S-0-FEM-E*	*Calculation of percentage change (increase(+) and decrease(-))%#*
Max. Load (KN)	***Push***	***218***	***103***	***-53***
	Pull	***-207***	***-109***	***-47***
Max. displacement (mm)	***Push***	***30***	***69***	***+130***
	Pull	***-26***	***-66***	***+154***
Stiffness (KN/mm)		***42.5***	***10***	***-77***
Cumulative Energy Dissipation (kN.m)		***4***	***0.7***	***-82.5***
Hysteresis Damping		***3.48***	***2.6***	***-25***

(#) percentage referenced to the specimen (S-01-FEM)

4.1.2 Effect of absence of concrete tie-columns

The following table 3 show the effect of absence of concrete tie-columns on the model, in case of the absence of concrete tie-columns in the model, the maximum load was decreased by 79%,78% for push and pull respectively ,the maximum displacement decreased by 90%, 89% for push and pull respectively, the stiffness decreased by 65%, the Cumulative Energy Dissipation controlled by maximum displacement of control model(S-01-FEM) decreased by99% and the Hysteresis Damping % controlled by maximum displacement of control model(S-01-FEM) decreased by16% .This study demonstrated the importance of concrete tie-columns for improvement of confined masonry building to resist the lateral loads, the concrete tie-columns transfer the model from brittle to ductile failure. Therefore, concrete tie-columns cannot be dispensed with, because they are considered one of the most important structural elements in confined masonry building.

Table. 3 –comparison of test results for model (S-01-FEM) and (S-01-FEM-M) in case of absence of concrete tie-columns.

		S-01-FEM	*S-01-FEM-M*	*Calculation of percentage change (increase(+) and decrease(-))%#*
Max. Load (KN)	***Push***	***218***	***45***	***-79***
	Pull	***-207***	***-45***	***-78***
Max. displacement (mm)	***Push***	***30***	***3***	***-90***
	Pull	***-26***	***-3***	***-89***
Stiffness (KN/mm)		***42.5***	***15***	***-65***
Cumulative Energy Dissipation (kN.m)		***4***	***0.03***	***-99***
Hysteresis Damping		***3.48***	***2.92***	***-16***

(#) percentage referenced to the specimen (S-01-FEM)

4.1.3 Effect of absence of out-plan walls

The following table 4 show the effect of absence of out-plan walls on the model, in case of the absence of out-plan walls in the model, the maximum load was decreased by 1.4% in case of push and increase by 2.9% in case of pull ,the maximum displacement decreased by 6.7%in case of push and increased by 7.7% in case of push ,the stiffness decreased by 1.2%, the Cumulative Energy Dissipation controlled by maximum displacement of control model(S-01-FEM) not changed and the Hysteresis Damping % controlled by maximum displacement of control model(S-01-FEM) not changed. This study demonstrated that the out-plan walls has no significant effect on the confined masonry building to resist the horizontal lateral loads.

Table 4 –comparison of test results for model (S-01-FEM) and (S-01-FEM-I) in case of absence of out-plan walls

		S-01-FEM	*S-01-FEM-I*	*Calculation of percentage change (increase(+) and decrease(-))%#*
Max. Load (KN)	***Push***	***218***	***215***	***-1.4***
	Pull	***-207***	***-213***	***+2.9***
Max. displacement (mm)	***Push***	***30***	***28***	***-6.7***
	Pull	***-26***	***-28***	***+7.7***
Stiffness (KN/mm)		***42.5***	***42***	***-1.2***
Cumulative Energy Dissipation (kN.m)		***4***	***4***	***0***
Hysteresis Damping		***3.48***	***3.48***	***0***

(#) percentage referenced to the specimen (S-01-FEM)

4.1.4 Effect of absence of in-plan walls

The following table 5 show the effect of absence of in-plan walls on the model, in case of the absence of absence of in-plan walls on the model, the maximum load was decreased by 47%,44% for push and pull respectively ,the maximum displacement increased by 147%, 169% for push and pull respectively, the stiffness decreased by 74%, the Cumulative Energy Dissipation controlled by maximum displacement of control model(S-01-FEM) decreased by 79% and the Hysteresis Damping % controlled by maximum displacement of control model(S-01-FEM) decreased by 28%. This study demonstrated the importance ofin-plan masonry walls for Effect of absence of in-plan walls main important structural element in design of confined masonry building.

Anyhow, figures 26.a to 26.e show the conclusion of this study to show the different affect for each case

Table. 5 –comparison of test results for model (S-01-FEM) and (S-01-FEM-O) in case of absence of out-plan wall

		S-01-FEM	*S-01-FEM-O*	*Calculation of percentage change (increase(+) and decrease(-))%#*
Max. Load (KN)	*Push*	*218*	*115*	*-47*
	Pull	*-207*	*-115*	*-44*
Max. displacement (mm)	*Push*	*30*	*74*	*+147*
	Pull	*-26*	*-70*	*+169*
Stiffness (KN/mm)		*42.5*	*11*	*-74*
Cumulative Energy Dissipation (kN.m)		*4*	*0.85*	*-79*
Hysteresis Damping		*3.48*	*2.5*	*-28*

(#) percentage referenced to the specimen (S-01-FEM)

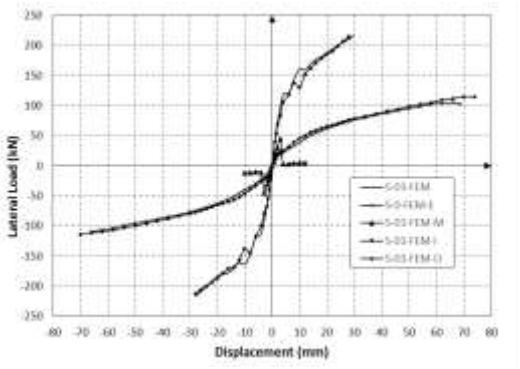

Fig 26.a – Envelope load-displacement curves for compared with model (S-01-FEM)

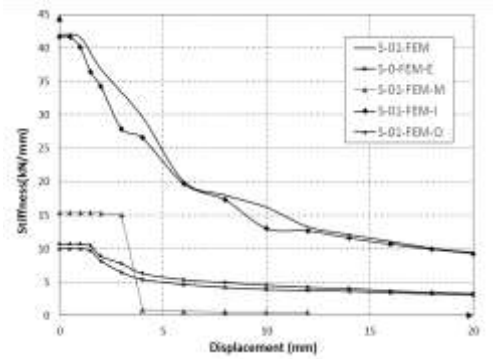

Fig 26.b. Stiffness curve for compared with model (S-01-FEM).

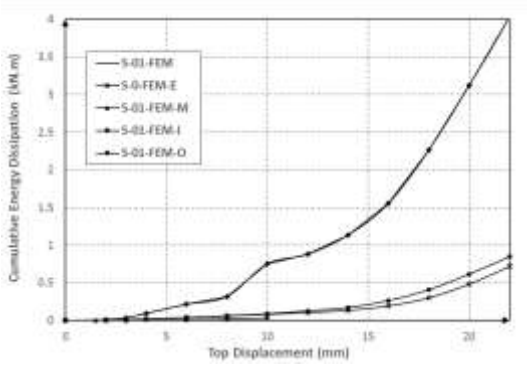

Fig 26.c Cumulative Energy Dissipation (KN.m) for compared with model (S-01-FEM).

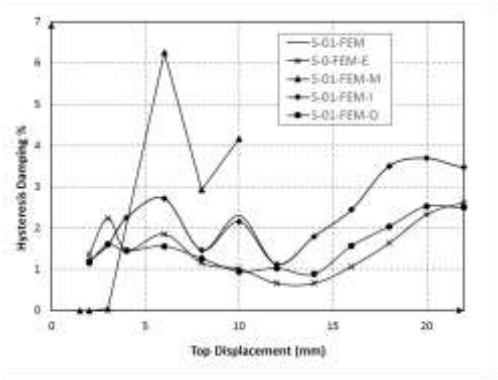

Fig 26.d. Hysteresis damping% for compared with model (S-01-FEM).

4.2 The of effect of In-plan and out-of-plan performance in case study (S-02-FEM)

4.2.1 Effect of absence of masonry walls

The following table 6 show the effect of absence of masonry walls on the model, in case of the absence of masonry walls in the model, the maximum load was decreased by 49%,48% for push and pull respectively ,the maximum displacement increased by 44%,38% for push and pull respectively the stiffness reduced by 69%, the Cumulative Energy Dissipation controlled by maximum displacement of control model (S-02-FEM) decreased by 56% and the Hysteresis Damping% controlled by maximum displacement of control model (S-02-FEM) decreased by 26% .This study demonstrated the importance of masonry walls for improvement of confined masonry building to resist the lateral loads and it's considered the main important structural element in design of confined masonry building.

Table 6 –comparison of test results for model (S-02-FEM) and (S-0-FEM-E) in case of absence of masonry walls.

		S-02-FEM	*S-0-FEM-E*	*Calculation of percentage change (increase(+) and decrease(-))%#*
Max. Load (KN)	*Push*	*203*	*103*	*-49*
	Pull	*-211*	*-109*	*-48*
Max. displacement (mm)	*Push*	*48*	*69*	*+44*
	Pull	*-48*	*-66*	*+38*
Stiffness (KN/mm)		*32.5*	*10*	*-69*
Cumulative Energy Dissipation (kN.m)		*18.7*	*8.3*	*-56*
Hysteresis Damping		*5.8*	*7.3*	*-26*

(#) percentage referenced to the specimen (S-02-FEM)

4.2.2 Effect of absence of concrete tie-columns

The following table 7 show the effect of absence of concrete tie-columns on the model, in case of the absence of concrete tie-columns in the model, the maximum load was decreased by 73%,74% for push and pull respectively ,the maximum displacement decreased by 92%, 92% for push and pull respectively, the stiffness decreased by 54%, the Cumulative Energy Dissipation controlled by maximum displacement of control model(S-02-FEM) decreased by 99% and the Hysteresis Damping % controlled by maximum displacement of control model(S-02-FEM) decreased by28% .This study demonstrated the importance of concrete tie-columns for improvement of confined masonry building to resist the lateral loads, the concrete tie-columns transfer the model from brittle to ductile failure. Therefore, concrete tie-columns cannot be dispensed with, because they are considered one of the most important structural elements in confined masonry building.

Table 7 – comparison of test results for model (S-02-FEM) and (S-02-FEM-M) in case of absence of concrete tie-columns

		S-02-FEM	*S-0-FEM-M*	*Calculation of percentage change (increase(+) and decrease(-))%#*
Max. Load (KN)	*Push*	*203*	*55*	*-73*
	Pull	*-211*	*-55*	*-74*
Max. displacement (mm)	*Push*	*48*	*4*	*-92*
	Pull	*-48*	*-4*	*-92*
Stiffness (KN/mm)		*32.5*	*15*	*-54*
Cumulative Energy Dissipation (kN.m)		*18.7*	*0.12*	*-99*
Hysteresis Damping		*5.8*	*4.18*	*-28*

(#) percentage referenced to the specimen (S-02-FEM)

4.2.3 Effect of absence of out-plan walls

The following table 8 show the effect of absence of out-plan walls on the model, in case of the absence of out-plan walls in the model, the maximum load was increased by 1.5% in case of push and decreased by 0.5% in case of pull ,the maximum displacement increased by 12.5%in case of push and not changed in case of push ,the stiffness decreased by 1.5%, the Cumulative Energy Dissipation controlled by maximum displacement of control model(S-02-FEM) decreased by 2% and the Hysteresis Damping % controlled by maximum displacement of control model(S-02-FEM) increased by 8.6%. This study demonstrated that the out-plan walls has no significant effect on the confined masonry building to resist the horizontal lateral loads.

Table 8 – comparison of test results for model (S-02-FEM) and (S-02-FEM-I) in case of absence of out-plan walls

		S-02-FEM	*S-0-FEM-I*	*Calculation of percentage change (increase(+) and decrease(-))%#*
Max. Load (KN)	*Push*	*203*	*206*	*+1.5*
	Pull	*-211*	*-210*	*-0.5*
Max. displacement (mm)	*Push*	*48*	*54*	*+12.5*
	Pull	*-48*	*-48*	*0*
Stiffness (KN/mm)		*32.5*	*32*	*-1.5*
Cumulative Energy Dissipation (kN.m)		*18.7*	*18.3*	*-2*
Hysteresis Damping		*5.8*	*6.3*	*+8.6*

(#) percentage referenced to the specimen (S-02-FEM)

4.2.4 Effect of absence of in-plan walls

The following table 9 show the effect of absence of in-plan walls on the model, in case of the absence of absence of in-plan walls on the model, the maximum load was decreased by 14%,19% for push and pull respectively ,the maximum displacement increased by 54%, 46% for push and pull respectively, the stiffness decreased by 63%, the Cumulative Energy Dissipation controlled by maximum displacement of control model(S-02-FEM) decreased by 36% and the Hysteresis Damping % controlled by maximum displacement of control model(S-02-FEM) decreased by 10%. This study demonstrated the importance of in-plan masonry walls for Effect of absence of in-plan walls main important structural element in design of confined masonry building. Anyhow, figures 27.a to 26.d show the conclusion of this study to show the different affect for each case.

Table 9 – comparison of test results for model (S-02-FEM) and (S-02-FEM-O) in case of absence of out-plan walls

		S-02-FEM	*S-0-FEM-O*	*Calculation of percentage change (increase(+) and decrease(-))%#*
Max. Load (KN)	*Push*	*203*	*175*	*-14*
	Pull	*-211*	*-171*	*-19*
Max. displacement (mm)	*Push*	*48*	*74*	*+54*
	Pull	*-48*	*-70*	*+46*
Stiffness (KN/mm)		*32.5*	*12*	*-63*
Cumulative Energy Dissipation (kN.m)		*18.7*	*12*	*-36*
Hysteresis Damping		*5.8*	*5.2*	*-10*

(#) percentage referenced to the specimen (S-02-FEM)

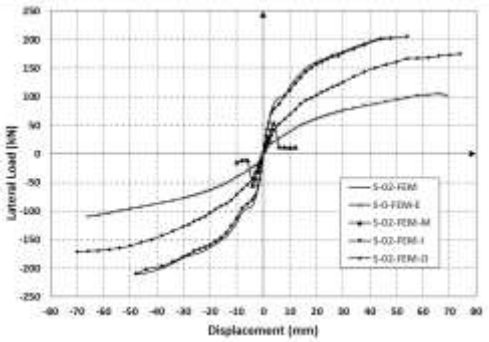

Fig 27.a – Envelope load-displacement curves for compared with model (S-02-FEM)

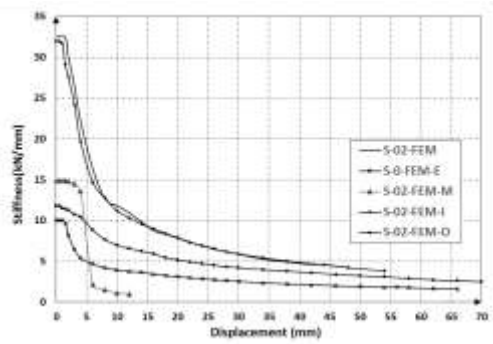

Fig 27.b. Stiffness curve for compared with model (S-02-FEM).

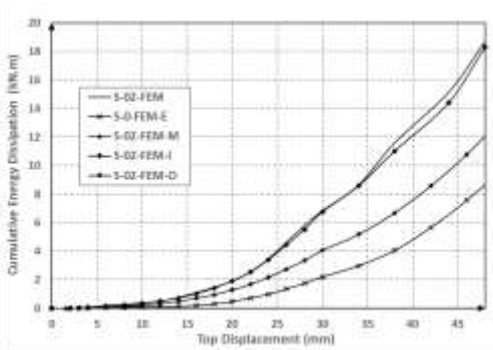

Fig 27.c Cumulative Energy Dissipation (KN.m) for compared with model (S-02-FEM).

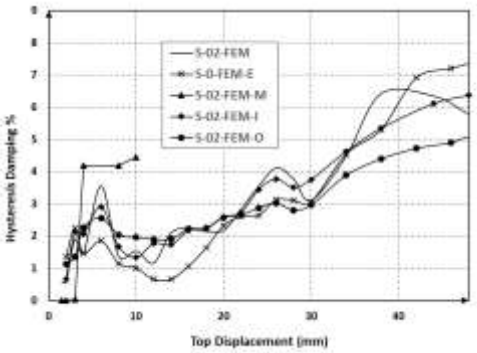

Fig 27.d. Hysteresis damping% for compared with model (S-02-FEM).

5.0 CONCLUSIONS

From the finite element study we get that the main findings of case study (S-01-FEM) can be noted as follows.

1. When has been studied without masonry walls, the maximum lateral horizontal load decreased by 50%, the drift increased by 142%, the initial stiffness decreased by 77% and cumulative energy dissipation decreased by 82%.
2. When have been without tie-columns, the maximum lateral horizontal load decreased by 78%, the drift decreased by 90%, the initial stiffness decreased by 65% and cumulative energy dissipation decreased by 99%there for the failure model transfer from ductile failure to brittle failure.
3. There is no significant effect in maximum horizontal load, drift, initial stiffness and cumulative energy dissipation when the model have been without out-plan walls.
4. When has been studied without in-plan walls, the maximum lateral horizontal load decreased by 45%, the drift increased by 58%, the initial stiffness decreased by 47% and cumulative energy dissipation decreased by 79%**.**

Also, from the finite element study we get that the main findings of case study (S-02-FEM) can be noted as follows.

1. When has been studied without masonry walls, the maximum lateral horizontal load decreased by 49%, the drift increased by 40%, the initial stiffness decreased by 69% and cumulative energy dissipation decreased by 56%.
2. When have been without tie-columns, the maximum lateral horizontal load decreased by 73%, the drift decreased by 92%, the initial stiffness decreased by 54% and cumulative energy dissipation decreased by 99%there for the failure model transfer from ductile failure to brittle failure.
3. There is no significant effect in maximum horizontal load, drift, initial stiffness and cumulative energy dissipation when the model have been without out-plan walls.
4. When the has been studied without in-plan walls, the maximum lateral horizontal load decreased by 17%, the drift increased by 58%, the initial stiffness decreased by 47% and cumulative energy dissipation decreased by 79%**.**

6.0 Reference

[1] E Abdulahad and E Mahmud et al. 2018. “Seismic behaviour before and after strengthening of solid confined masonry walls with glass fiber reinforced polymers - analysis of hysteresis curves, obtained by shaking table tests”

[**2**] Borah, Bonisha & Kaushik, Hemant & Singhal, Vaibhav. (2020). Finite Element Modelling of Confined Masonry Wall under In-plane Cyclic Load. 10.1088/1757-899X/936/1/012020.

[**3**] Hatzinikolas, Michael & Korany, Yasser & Brzev, Svetlana. (2015). Masonry Design for Architects and Engineers. Canadian Masonry Publications ISBN: 978-0-9780061-1-2

[4] Roberto M., Brzev S., Maximiliano A., Teddy B., Francisco C., Junwu D., Mohammed F., Tim H., Ahmed M., Moghadam A., Daniel Q., Tomazevic M., Luis Y. (2011).”Seismic design guide for low-rise confined masonry buildings

[5] J. Martin Leal-Graciano, Basilia Quiñónez, Héctor E. Rodríguez-Lozoya, Juan J. Pérez-Gavilán, José F. Lizárraga-Pereda, Use of GFRP as retrofit alternative for confined masonry walls with window opening subjected to in-plane lateral load, Engineering Structures, Volume 223, 2020, 111148, ISSN 0141-0296,

[6] Mosaad El-Diasity, Hussein Okail, Osama Kamal, Mohamed Said, Structural performance of confined masonry walls retrofitted using ferrocement and GFRP under in-plane cyclic loading,Engineering Structures, Volume 94, 2015, Pages 54-69, ISSN 0141-0296.

[7] Hemant B. Kaushik1; Durgesh C. Rai2; and Sudhir K. Jain, (2007), “Stress-Strain Characteristics of Clay Brick Masonry under Uniaxial Compression”, Journal of Materials in Civil Engineering, Vol. 19, No. 9, ASCE, pp. 728-739.

[8] Huang Yan, Kan Minghui, and Wang Zifa,(2011), “Nonlinear analysis for monotonic and low

cyclic loading" Applied Mechanics and Materials, 94-96, pp. 406-415.

[9] ANSYS® Academic Research, Release 15.0, ANSYS, Inc

[10] El-Dakhakhni, W. (2002). *Experimental and analytical seismic evaluation of concrete masonry - infilled steel frames retrofitted using GFRP laminates* (Order No. 3061128). Available from ProQuest Dissertations & Theses Global. (304803971). Retrieved from https://www.proquest.com/dissertations-theses/experimental-analytical-seismic-evaluation/docview/304803971/se-2?accountid=178282

[12]Jhair Yacila, Guido Camata, Jhoselyn Salsavilca, Nicola Tarque,Pushover analysis of confined masonry walls using a 3D macro-modellingapproach,EngineeringStructures,Volume 201,2019,109731,ISSN 0141-0296

[13] Tomazevic, M., and Klemence, I. (1997)."Verification of seismic resistance of confined masonry buildings."Earthquake engineering and structural dynamics, Vol. 26, 1073-1088

[14] Safarizki, Hendramawat & Marwahyudi, Marwahyudi. (2021). Determining initial damage state of confined masonry wall. Journal of Physics: Conference Series. 1912. 012058. 10.1088/1742-6596/1912/1/012058.

[15] Smoljanović H, Živaljić N, Nikolić Ž and Munjiza A 2017 Numerical model for confined masonry structures based on finite discrete element method Int. J. for Engg. Modelling 30(1-4) 19–35

[16] Yacila J, Camata G, Salsavilca J and Tarque N 2019 Pushover analysis of confined masonry walls using a3d macro-modelling approach Engg. Struct. 201 109731

[17] Janaraj T and Dhanasekar M 2014 Finite element analysis of the in-plane shear behaviour of masonry panels confined with reinforced grouted cores Const. and Build. Mat. 65 495–506